Computable Invariants of Links in the Three-torus

Sahar Masoudian

A thesis submitted for the degree of
Master of Philosophy at
The Australian National University

June 2020

Except where otherwise indicated, this thesis is my own original work.

Sahar Masoudian
15 June 2020

To my dear mother

Acknowledgments

I have made efforts in this thesis. However, the completion of this study could not have been possible without the expertise of Dr. Vanessa Robins.

I would also like to express my gratitude towards my parents and friends for their kind support and encouragement during doing this thesis.

Abstract

This work contributes to our knowledge of a type of crystal called rod packings by viewing them as links in the three-torus and computing the fundamental group of their complementary space, which is a topological invariant for these structures.

Topological notions play an important role in chemistry. Chemists need the topological properties of crystalline materials for better understanding of their connectivity and classification [Ockwig et al., 2005].

We extend some standard invariants in knot theory from the normal case of knots and links in $\mathbb{S}^3$ to the case of knots and links in $\mathbb{T}^3$. The fundamental group of the complement of knots and links is selected in this study. Although this invariant is not a complete invariant as we show in Chapter 3, it is still a strong invariant to compute. It is possible to compute this invariant by hand for simple examples in this thesis, and there are practical algorithms for computing the presentation of more complicated examples such as helical weavings [Evans et al., 2013].

We compute this invariant to classify the structures described in O'Keeffe et al. [2001] topologically, then we compare our equivalency classes with ambient isotopy of weavings [Evans et al., 2013] produced by a physical simulation for these periodic structures (called PB-SONO algorithm). In Grishanov et al. [2009], doubly periodic structures are considered for computing some numerical invariants, which leads us to enumerate some easier invariants such as the number of components. However, these invariants are not sufficient to discriminate the 3-periodic structures in our case, since some of them have the same invariants. For our computations, we use the standard techniques in knot theory from Rolfsen [1976] and some works on the topology of the three-torus from Johnson [2006].

As it was mentioned, we compute the fundamental group of the complement of these links (structures from crystallography). This invariant is sufficient to prove these structures are distinct within the 3-torus. Then we generalise the example of Whitehead links [Whitehead, 1937] in the 3-torus by using a twisting homeomorphism in a handlebody (with boundary of P-surface) from the standard Heegaard splitting of the 3-torus. This shows that the complementary space is not a complete invariant for links in the 3-torus.

Contents

List of Figures

List of Tables

Chapter 1

Introduction

In crystallography, some structures are naturally modelled by arrangements of non-intersecting cylinders [O'Keeffe and Andersson, 1977].The number of possible cylinder packings is infinite, but O'Keeffe et al. [2001] showed that if we restrict to structures with cubic symmetry whose cylinder locations are fixed by their symmetry group (i.e. there are no free parameters), then there will be six cylinder packings, and these packings have their axis directions either parallel to the coordinate axes, or to the body-diagonals, as shown in Figure (1.1).

Each cubic cell represents the concept of identification of the three-torus in the universal covering space $\mathbb{R}^3$; in this respect, these six invariant cylinder packings can be seen as entangled structures in $\mathbb{T}^3$. Each axis becomes a single component of these entanglements; then by identification of opposite faces of the cube, one can get an embedding of a circle along the cylinder axis. In this sense, we have multiple copies of embeddings of $\mathbb{S}^1$ in the 3-torus, which represent links in this manifold.

From knot theory, there are some properties (invariants) which stay the same under continuous deformations. The complement of these links in $\mathbb{T}^3$ is one such property to distinguish them, and a computable way to quantify this invariant is calculating the fundamental group of these complements. By applying the Van-Kampen theorem [Hatcher, 2001], we compute the fundamental group of the complement of these links manually. Then by counting the number of low index subgroups [Fleming, 2016] for at least index 3, one can conclude that all these computed fundamental groups are non-isomorphic groups. As a result of these computations, the in-equivalency between these structures as links in the 3-torus can be proved.

But the question of whether the complementary space completely determines the isotopy class of a link in $\mathbb{T}^3$ is still unclear. We address this problem by generalising the example of Whitehead links [Rolfsen, 1976] with homeomorphic complements and twisting homeomorphism on Heegaard handle-body in the standard Heegaard splitting for the 3-torus. We construct two distinct links with two components, where one of them bounds a disk in $\mathbb{T}^3$ (unknot component), with homeomorphic complements in Chapter 4. The example shows the complementary space is not a complete invariant.

At the end, with the above computations the following state will be proved:

The six cylinder packings with invariant position of axes in cubic symmetry in O'Keeffe et al. [2001], where the axes are along directions either $[111] or [100]$, are all

inequivalent links in the three-torus ($\mathbb{T}^3$).

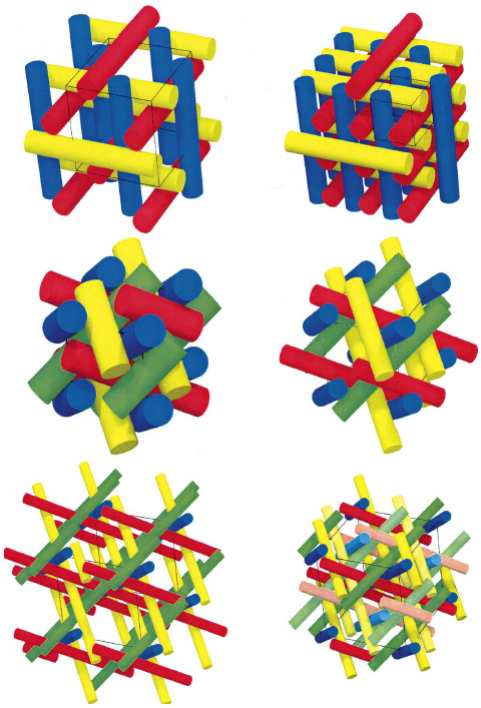

Figure 1.1: The six invariant cylinder packings. Top row: left ${}^{+}\Pi$, right $\Pi^{\star}$. Middle row: left Γ, right ${}^{+}\Omega$. Bottom row: left ${}^{+}\Sigma$, right: $\Sigma^{\star}$ (figure courtesy of O'Keeffe et al. [2001])

1.1 Thesis outline

We have four chapters in this thesis. We explain the motivation behind this study, some basic definitions, and a brief history of this work in Chapter 2. Then in Chapter 3, the methodology used in this study for the computations of the fundamental groups is addressed. Finally to compare these derived algebraic groups, GAP, which is a programming language for computational discrete algebra, is used to prove that these fundamental groups are distinct. In Chapter 4, the background and the history of the complement of knots and links in $\mathbb{S}^3$ are represented; then we generalise the conclusion of Whitehead [1937] for the links in the three-torus which cannot be determined by their complementary space in this 3-manifold. In this regard, the fundamental group of the complement of links in the three-torus is not a complete invariant. By this process, we will obtain the proof of the main theorem in Chapter 5.

Chapter 2

Background and Related Work

2.1 Motivation

The general target of this study is to compute invariants of periodic structures in 3-space, which can be seen as knots or links in the three-torus $\mathbb{T}^3$. The focus of this part of the work is cylinder packings, that are special type of periodic structures and the simplest examples for computations because they do not have complex twisting or knotted curves in each component. Now we explain more details about these periodic structures and the benefit of our computations.

Understanding, designing, and compounding chemical structures is of great significance in material sciences. Modelling these structures allows scientists to design and synthesize new materials. Some chemical structures are modelled by packing infinite cylinders that represent atoms bonded in rod-like chains, and are invariant under three independent translation vectors in 3-dimensional space [O'Keeffe and Andersson, 1977]. When modelling chemical structures, it is desirable to classify them according to different criteria in order to be able to distinguish equivalent classes. Researchers have developed physically based equivalency classes for some of these building units [Evans et al., 2015]. However, the enumeration of these periodic structures is still incomplete as there isn't yet a fully systematic method for enumerating periodic knots and links up to some level of complexity. In this regard, the motivation of this study is finding methods to determine when certain crystal structures might be equivalent or inequivalent in both physical and mathematical senses, as such the concept of equivalency in terms of both physics and mathematics will be explained. To understand how structures can be grouped into a class, first the periodic structures themselves are described.

Crystal structure is the description of the ordered arrangement of atoms, ions, and molecules, which are studied in an experimental science called crystallography. Naturally, these ordered structures have symmetries that repeat along three different directions of the three dimensional space. The description of these arrangements and symmetries of crystals are encoded by space groups. Cylinder packings are one type of crystal structure which we investigate here. Invariant cubic cylinder packings with non-intersecting cylinder axes were expressed by O'Keeffe et al. [2001] in six number of these structures. The invariant position of cylinder axes means that

no coordinate parameters for the position of the rods can be varied independently. These six invariant cylinder packings become links in $\mathbb{T}^3$. To develop the equivalency classes of these structures, we first need to know when two such structures are equal.

For classification and enumeration of crystal structures, one important issue is understanding whether some of the crystalline structures are equivalent or inequivalent. However, there are many different ways to define equivalency. Consider the basic structural unit of all silicate minerals is the silicon tetrahedron in which one silicon atom is surrounded by and bonded to four oxygen atoms, and each of these oxygen atoms belongs to two silicon tetrahedra. Different minerals can be classified according to different features.

For instance, chemical equivalency is about stoichiometry or the proportion of atoms of each type, and in this sense all silicate minerals are the same. Then we could mention geometric equivalency which usually means rigid body motions (translation, glide, rotation); in this sense silicate minerals can be different by the specific position of atoms within a space group.

In terms of topology, two equivalent structures are two structures that can be mapped to each other continuously; this continuous mapping permits bending and twisting but not tearing or gluing, and is called a homeomorphism. Officially, we write $X \cong Y$ if there is a homeomorphism ϕ which maps X to Y. In this sense of equivalency, SiO_4 tetrahedral units can share oxygen atoms and be linked in a variety of ways, which result in different structures. Therefore, different minerals are classified according to their different arrangements of tetrahedra and their links. Equivalency in knot theory (for 3-space) is stronger so that the homeomorphism is of the space they are embedded in, as in Definition 2. In knot theory (the study of mathematical knots), distinct knots and links are recognized by computing their invariants. These homeomorphisms are specifically for $\mathbb{R}^3$, but the general concept of equivalency is ambient isotopy, and because we consider crystals in the three-torus, only ambient isotopy is considered as an equivalency relation.

An invariant is any quantitiy that is preserved under ambient isotopy. Generally, if two structures have distinct invariants, they are inequivalent, but having equal invariants does not necessarily make structures equal. Similarly, equivalent crystalline structures should be related to their invariants (for example the complementary space of them), because they actually become knots or links in a special topological space called the three-torus $\mathbb{T}^3$ (Section 2.5). The three-torus is the quotient space of $\mathbb{R}^3$ modulo the translation symmetry group. In fact, crystal structures are infinite periodic structures in $\mathbb{R}^3$, but by assuming them as the entangled structures in the compactified unit cell, we make the calculations of their group presentation finite. As mentioned before, the focus of this work is to compute one type of invariant for cylinder packings, and these structures are links in this topological space. Now we explain the reasons to consider topological equivalency or inequivalency in this study, and select a very specific invariant to determine this.

In chemistry, topology provides a simple way of describing and predicting the overall structure of molecules. For logical synthesis (chemical synthesis) of crystal structures or for predicting their connectivity (chemical bonds), we need their under-

lying topological properties. For example, Ockwig et al. [2005] deduced a method to classify metal-organic frameworks (MOF) by using the topology of their nets, so they simplified or reduced the number of analysed MOF structures belonging to the same type of net topologies (net is a periodic geometric graph in $\mathbb{R}^3$ that is abstract structure of atoms in a crystal). 1127 MOFs were studied by Ockwig et al. [2005] from the Cambridge Structural Database (CSD). 774 MOFs have net topology with a single vertex degree (coordination number). Out Of these, over 60% have net topology identified as belonging to the simplest and most-symmetric uninodal nets ("the regular nets" described in Friedrichs et al. [2003]).

There are a variety of different types of invariants for knots and links. The simplest is the number of components of links. However, this invariant is the same for many rod packings in this study in the specific primitive unit cell, see Table (2.2). More complicated invariants are the various knot polynomials [Kauffman, 1993] which are based on 2D projections, and would require substantial mathematical machinery to generalise to the periodic case [Grishanov et al., 2009]. In Section 2.3 we mentioned that the complementary space of finite knots and links in $\mathbb{R}^3$ (or $\mathbb{S}^3$) is recognized as an object which is preserved under ambient isotopies. This invariant becomes more computable via the fundamental group, which is our interest to compute.

In this study, we will compute the fundamental groups of the complementary space of the invariant cylinder packings per unit cell, and prove that the six invariant cylinder packings are non-isotopic (inequivalent) links in $\mathbb{T}^3$. This finding is the first step to find out more about computable invariants of links in the three-torus, where it is important to develop the methods during this thesis.

2.2 Fundamental groups

In this section, we explain the importance of computing the fundamental groups of general topological spaces.

The equivalency relation between paths in mathematics is defined by homotopy relations. Consider two paths with the same endpoints; if there is a continuous deformation between these two paths, we say they are homotopic. Being continuous means one cannot exclude (for example) a point from the region between two paths. This continuous deformation is called homotopy map. Below is the official definition in mathematics.

Definition 1 *Suppose f_0 & $f_1 : I = [0,1] \to X$ are two paths in a topological space X, with the start point $f_0(0) = f_1(0) = x_0$ and the end point $f_0(1) = f_1(1) = x_1$. They are homotopic if there is a continuous map $F : I \times I \to X$ such that $F(x,t) = f_t(x)$, where f_t is the family of homotopy of paths in X. (see Figure(2.1))*

$$\begin{cases} F(0,t) = x_0 \\ F(x,0) = f_0(x) \\ F(x,1) = f_1(x) \\ F(1,t) = x_1 \end{cases}$$

Now we need to have an operation for (equivalence classes of) paths as we want to

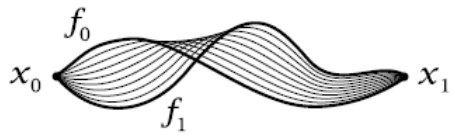

Figure 2.1: Two homotopic paths f_0 and f_1 with the same endpoints x_0 and x_1, and we write $f_0 \cong f_1$ [Hatcher, 2001]

define a group. This operation is the composition of paths, which is shown by $f \bullet g$, and it is simply to traverse f, then g. The following is the official formula by which this composition is defined

$$f \bullet g = \begin{cases} f(2t) & 0 \leqslant t \leqslant \frac{1}{2} \\ g(2t-1) & \frac{1}{2} \leqslant t \leqslant 1 \end{cases}$$

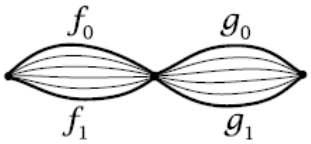

Figure 2.2: The composition of f_0 and g_0 is homotopic to the composition of f_1 and g_1, or $f_0 \bullet g_0 \cong f_1 \bullet g_1$ [Hatcher, 2001]

Now assume f and g are loops in X, i.e. $f(0) = g(1) = x_0 = f(0) = g(1)$ (meaning the start and end points are the same). We define elements of a group to be the homotopy equivalence classes of loops with basepoint x_0, and the group product to be path composition. This object is the fundamental group of X with basepoint x_0, denoted $\pi_1(X, x_0)$. The fundamental group of a topological space with two different basepoints are isomorphic, so one can take any basepoint.

The fundamental group plays an important role in discriminating between the topological spaces. If two topological spaces have non-isomorphic fundamental groups, these are not homeomorphic spaces. Although computing the fundamental groups and comparing them is not always easy, there are some tools we can use for this goal, which will be introduced in Section 2.3.1 and Theorem 3.

Now, we know the elements of fundamental groups are loops, but during computations one must be careful about loops which are homotopic. Two loops with the same basepoint are regarded as determining the same element of the fundamental

group of X if one loop can be continuously deformed to the other within space X. For example, suppose X is the complement of the circle A in $\mathbb{R}^3$ shown in Figure (2.3), then the composition of two loops $a \cdot b$ in that figure is deformable to c, with respect to the direction which is shown in Figure (2.3). We will describe how we tackle the problem of computation of fundamental group of the complement of a given knot or link in $\mathbb{R}^3$ by using the Wirtinger presentation method in section 2.3.

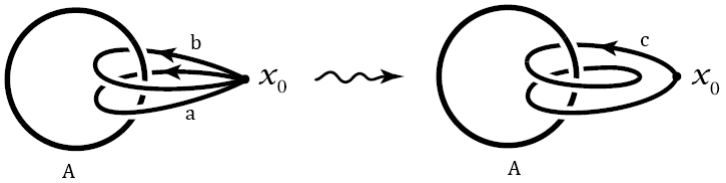

Figure 2.3: Two deformable elements in fundamental group of $X = \mathbb{R}^3 \setminus A$ (figure courtesy of Hatcher [2001])

2.3 Knots and Links

In this section, we review some definitions and theorems corresponding to knots and links. We also describe how to determine knot types by their complements, which we need for computations in Chapter 3.

Definition 2 *A Knot is the embedding of S^1 in a 3-manifold M^3 and a link is the embedding of the disjoint union of k copies of S^1 in a 3-manifold.*

Two knots or links are equivalent (ambient isotopic) if there is a homeomorphism

$$F : M^3 \to M^3$$

which is isotopic to the identity and maps one knot to the other one.

Any orientation preserving homeomorphism in $\mathbb{R}^3$ is smoothly isotopic to the identity Lickorish [2012]. Therefore, we can express the equivalency of knots and likns in $\mathbb{R}^3$ as the following.

Two knots or links K_0&K_1 in $\mathbb{R}^3$, are ambient isotopic (equivalent, or $K_1 \cong K_2$) if there is an orientation preserving homeomorphism on $\mathbb{R}^3$, ϕ, that maps K_0 to K_1 ($\phi(K_1) = K_2$).

Any properties of a knot that are preserved under ambient isotopy is known as an invariant of a knot (or link).

This equivalency means those knots or links which are equivalent, can be deformed to each other. All these deformations can be reduced to a sequence of three moves called Reidemeister moves; see Figure (2.5). As an example of equivalent knots, we present one hard unknot (unknots in M^3 must bound a disk) which can be deformed to a simple unknot by the following diagram showing a sequence of Reidemiester moves. This unknot is called “Culprit" [Kauffman and Lambropoulou, 2012], and can be seen in Figure (2.6).

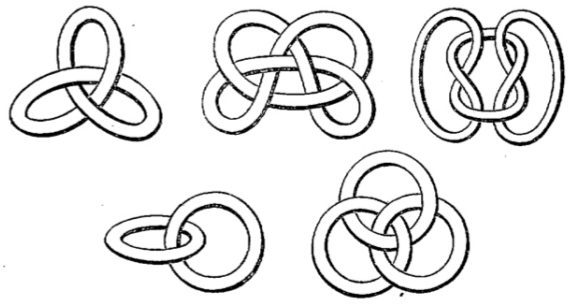

Figure 2.4: Examples of knots and Links (Kauffman [1993])

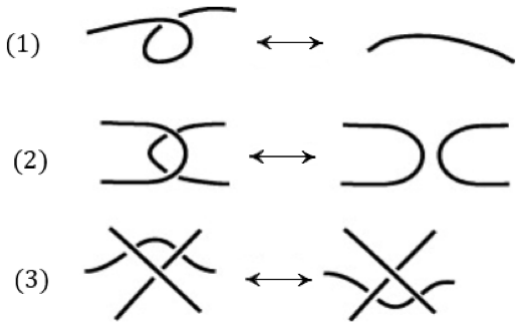

Figure 2.5: Three Reidemeister moves, or equivalence moves

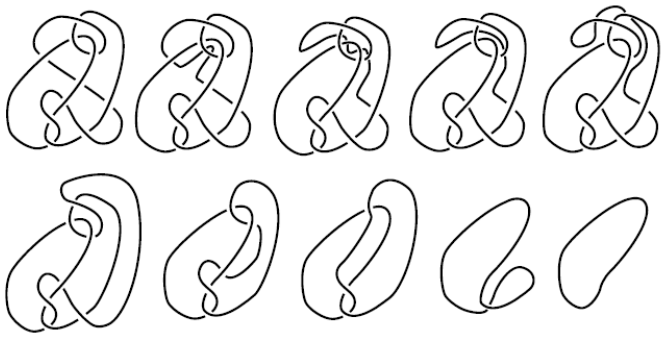

Figure 2.6: The Culprit diagram (Kauffman and Lambropoulou [2012])

It follows from Definition 2 that the complementary spaces of two equivalent knots or links in $\mathbb{R}^3$ or an arbitrary 3-manifold must be also equivalent, i.e. homeomorphic [Raymond, 1997]; we therefore have the following theorem:

Theorem 1 *If $K_0, K_1 \subset M^3$, are two equivalent knots in M^3, then $\pi_1(M^3 \setminus K_0) \cong \pi_1(M^3 \setminus K_1)$.*

Consequently, one example of an invariant in knot theory is the fundamental group

of the complementary space of the knot or link, called the knot group for short. If two knots or links K_0 and K_1 have non-isomorphic fundamental groups, then K_0 and K_1 are not isotopic.

It has been proved that the complementary space of a knot in $\mathbb{S}^3$ is a complete invariant [Gordon and Luecke, 1989]. In other words, if the complementary spaces of two knots are related to orientation preserving homeomorphism, then the knots are ambient isotopic. However, the knot group is complete only for prime (indecomposable) knots in $\mathbb{S}^3$ [Whitten, 1987]. Nevertheless, neither of these results apply to links in the 3-sphere [Rolfsen, 1976]. We will discuss more about knots and links that can be determined by their complementary space in Chapter 4.

2.3.1 Wirtinger Presentation

In this section, we explain a systematic method from Rolfsen [1976] for computing a presentation of the fundamental group of the complement of a given knot or link in $\mathbb{R}^3$.

First, let the basepoint of the knot (or link) group be $x_0 = (0, 0, 1)$(this base point is not on the knot). The basepoint x_0 should be thought of as the eye of the beholder. Any knot or link can be given by a projection onto the plane with no multiple points more than double. These double points are called crossings. We break at each crossing to obtain a finite set of arcs C_i, and $\pi_1(\mathbb{R}^3 \setminus K)$ is generated by loops c_i which pass around these arcs shown in Figure (2.7). Therefore, the number of crossings determines the number of generators. Also from Section 2.2, we now know one can find an expression for the loop that circles around underneath the four arcs near a crossing in terms of the loops around those four arcs. This loop must come from the basepoint, and then go back to x_0. We choose an orientation for the knot, and then orient the generators c_i around the arcs by right-hand screw convention (RHR).

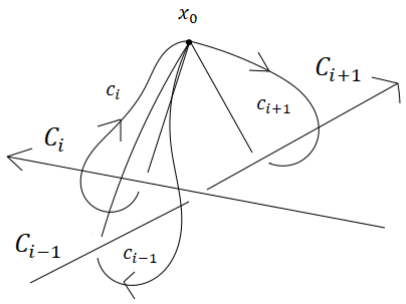

Figure 2.7: Loops or generators which go underneath with the direction regards to right-hand rule for a given crossing of a knot or link

For example in Figure (2.8), we can see that for crossing (1) in trefoil knot the curve $c_{i+1}^{-1} c_i c_{i-1} c_i^{-1}$ contracts to a point, so we have the relation $c_{i+1}^{-1} c_i c_{i-1} c_i^{-1} = id$ between generators. By selecting another direction for the knot, the presentation of the

complementary space of knot would not be changed which means this presentation is independent of knots direction.

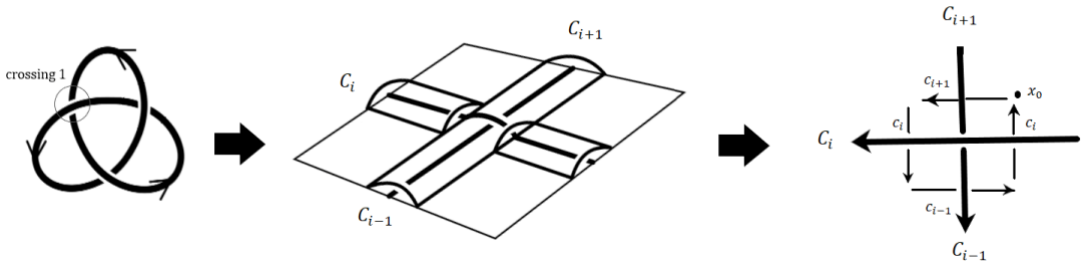

Figure 2.8: Wirtinger relation for the diagram of a crossing number 1, where the relation is written from x_0 then goes underneath and follows the arrows, then goes back to the basepoint. Use RHR for the power of c_is whether it is $+1$ or -1.

Theorem 2 *Suppose K is a knot in* $\mathbb{R}^3$ *with n crossings. The group* $\pi_1(\mathbb{R}^3 \setminus K)$ *is generated by the(homotopy classes of the)* c_i *and has presentation*

$$\pi_1(\mathbb{R}^3 \setminus K) =< c_1, ..., c_n | r_1 \dots r_n >$$

Moreover, a single r_i *may be omitted and the above remains true[D.Rolfsen,1976].*

More explanation and the proof of this theorem has been presented in Rolfsen [1976].

2.4 Linking Number

One invariant of 2-component links is the linking number.

Definition 3 *In an oriented diagram of a link, all crossings (double points in the diagram) can be positive* ($\varepsilon = +1$) *or negative* ($\varepsilon = -1$) *according to Figure (2.9)*

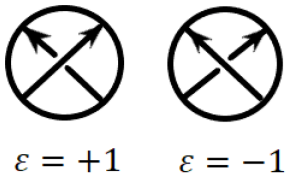

Figure 2.9: Crossing signs for oriented diagrams

The sum of all positive crossing signs minus all negative crossing signs is equal to twice the linking number. For example, the linking number of Hopf link in Figure (2.10) is one.

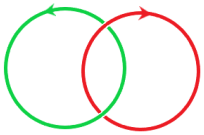

Figure 2.10: Hopf link

2.5 Three-torus

The three-torus is a 3-manifold with the fundamental group $\mathbb{Z}^3$. Before any explanation for the three-torus, we consider the lower dimensional one which is the two-torus shown in Figure (2.11). We know $\mathbb{R}^2$ is the universal covering space for $\mathbb{T}^2$ [Hatcher, 2001], so it is possible to transform a planar diagram of $\mathbb{T}^2$ to its periodic unit square over $\mathbb{R}^2$. This completely defines the topology of any 2-periodic structure which has been applied in textile industry [Grishanov et al., 2009]. Different weaves and knits become knots or links in the two-torus. A two-dimensional pattern which is known as plain weave textile pattern is shown in Figure (2.12).

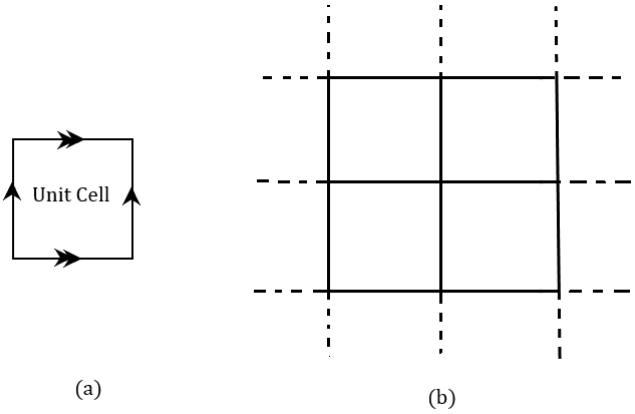

Figure 2.11: (a): Planar diagram of the two-torus, (b): Periodic unit cell in $\mathbb{R}^2$, which is another representation of $\mathbb{T}^2$

Figure 2.12: A two dimensional periodic pattern called Plain Weave in the unit cell [Grishanov et al., 2009]

Now we obtain the three-torus by starting with a solid cube in $\mathbb{R}^3$, and identifying opposite faces; see Figure (2.13). Again the universal covering space of this

3-manifold is $\mathbb{R}^3$, so we can have the periodic cube in the 3-space. In this regard, any periodic tangled structure without intersection point in its filaments, similar to Figure (2.14), can be considered as a knot or link in the three-torus.

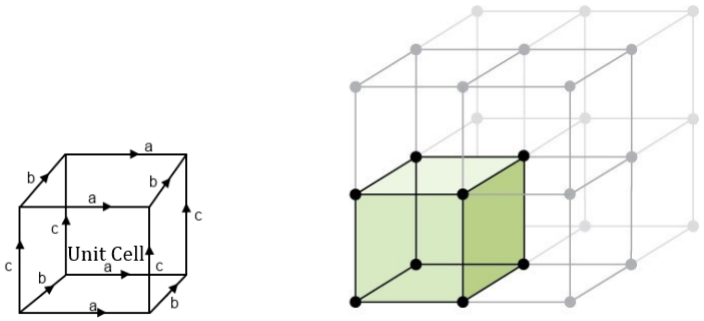

Figure 2.13: (a): Solid cube for which the opposite faces are identified, (b): Periodic unit cell in $\mathbb{R}^3$, which is another representation of $\mathbb{T}^3$

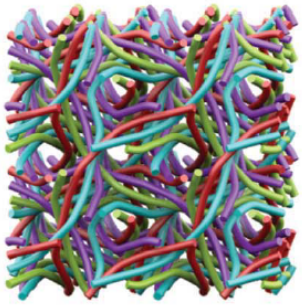

Figure 2.14: Example of a periodic tangled structure in the three-torus [Evans et al., 2015])

Now we want to use the definition of quotient space to define $n-$ torus in general.

Definition 4 . *The orbit space $\mathbb{R}^n / L$ or the lattice space, is $\{[x]|x \cong x + l(x \in \mathbb{R}^n, l \in L)\}$, where*

$$L = \{\Sigma_{i=1}^{m} k_i a_i | k_i \in \mathbb{Z}, a_i \in \mathbb{R}^n\}$$

$\{a_i\}$ are m vectors that span $\mathbb{R}^n$. In other words, the periodic patterns of points in $\mathbb{R}^n$ are the lattice spaces. Now, the following definitions are required for this quotient space

- A primitive unit cell(or a fundamental domain) is a parallelepiped with the generators $\{b_i\}_{i=1}^{n}$ such that b_i is a basis for $\mathbb{R}^n$ and generates L;

$$P = \{x | x = \sum_{i=1}^{n} t_i b_i, 0 \leqslant t_i \leqslant 1\}.$$

- A non-primitive unit cell is another parallelepiped with the generators $\{d_i\}_{i=1}^n$*, where* d_i *is still a basis for* $\mathbb{R}^n$*, but* d_i *generates a subgroup of L.*

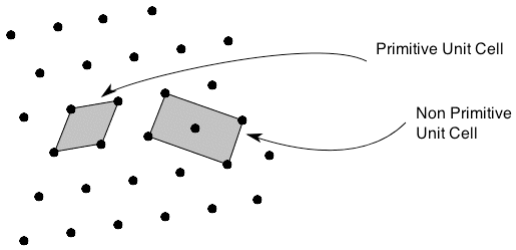

Figure 2.15: Two different cells for a 2D-pattern

Both types of cells are used to describe the symmetry and the structure of lattices. The primitive unit cell is useful because it is a fundamental domain (minimal region of space that is needed to fill $\mathbb{R}^n$ by the lattice translation, see Section 2.7.1). Although the basis vectors for non-primitive unit cells don't generate full lattice, they are used in crystallography when they are generated by orthogonal vectors, or display the rotational symmetries of the lattice more clearly than a primitive unit cells.

The quotient space of $\mathbb{R}^n$ modulo the translation symmetry group is the n-torus or $\mathbb{T}^n$. symmetry group of an object is the group of all transformations under which the object is invariant, and the translation symmetry group means that the object is invariant under any movements, a shift or a slide, but not a rotation or a reflection.

2.6 Cylinder Packings

Crystalline structures are a model of the ordered natural arrangements of particles such as atoms, ions, and molecules to form symmetric patterns in $\mathbb{R}^3$. In definition 4 when $n = 3$, lattice spaces can represent the interior of crystalline materials. The particular part of these patterns that constitute the repeating pattern are the unit cells in definition 4 which express the translational symmetry of the entire crystalline structure. This translational symmetry permits mathematical modelling of the crystal's physical properties as it means we can easily specify the location of, for example, an entire mole of atoms (6×10^{23}). In other words, one can get the whole structure by repetitive translation of the unit cell along the three different directions of the three dimensional space. The Bravais lattices are distinct types of lattices grouped according to the symmetries of the point pattern generated by a single point at each integer combination of generating vectors. In $\mathbb{R}^3$, there are 14 Bravais lattices. These are obtained by combining one of the seven lattice systems (Triclinic, Monoclinic, Orthorhombic, Tetragonal, Rhombohedral, Hexagonal, and Cubic) with one of the centering types. The centering types identify the locations of the lattice points in the unit cell as follows:

- Primitive (P): lattice points on the cell corners only (sometimes called simple).

- Base-centered (A, B, or C): lattice points on the cell corners with one additional point at the center of each face of a pair of parallel faces of the cell (sometimes called end-centered).
- Body-centered (I): lattice points on the cell corners, with one additional point at the center of the cell; see Figure 2.16.
- Face-centered (F): lattice points on the cell corners, with one additional point at the center of each of the faces of the cell.

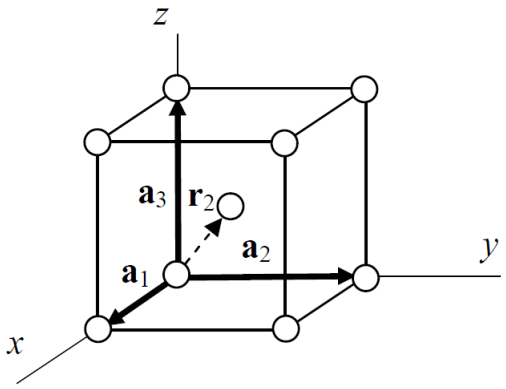

Figure 2.16: Example of a Body-centered cubic lattice with 4 translation vectors $\{a_1, a_2, a_3, r_1\}$ [Tsymbal]

The symmetry of all crystalline structures are encoded by space groups. Now we define one example of a crystalline structure: cylinder (or rod) packings.

Definition 5 *Crystalline cylinder (rod) packings are three-dimensional structures with translational symmetry that are modelled by infinitely long non-intersecting curves. The simplest cases are those where the curves are straight lines and each axis is mapped to the other by a symmetry of the whole structure [O'Keeffe and Andersson, 1977].*

Crystallographers generally divide whole different types of the above structures into three different general groups according to the different cylinder axis directions; then in each group, one can expand the number of structures by varying symmetry, density of occupied cylinders, or adding more rods. The most noticeable difference between this taxonomy of cylinder packings is that axes of cylinders will span different dimensions of space. This means that in each case, the translation vectors for the rod packings span different spaces $\mathbb{R}^n$ (see Table 2.1).

In the last type in Table (1), six packings of symmetry-related cylinders are described by O'Keeffe et al. [2001] with axes in invariant (special) positions (shown in Figure 1.1). Two of them have axes with direction vectors parallel to $[1,0,0]$, $[0,1,0]$, or $[0,0,1]$, or $\langle 100 \rangle$ in Miller index notation, and four of them have axes along $\langle 111 \rangle$ directions [O'Keeffe et al., 2001]. For the two sets with the positions of the cylinders

Type of cylinder packings	Figure of an example
Parallel axes (set of all direction vectors spans $\mathbb{R}^1$)	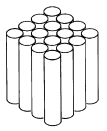
Parallel planes (set of all direction vectors spans $\mathbb{R}^2$)	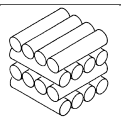
Not coplanar (set of all direction vectors spans $\mathbb{R}^3$)	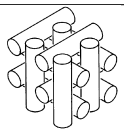

Table 2.1: Three types of cylinder packings [O'Keeffe and Andersson, 1977]

in $\langle 100 \rangle$ directions, the parametric equations of axes within the cubic unit cell for each structure are

$$\Pi^\star = \{(\frac{1}{2}, 0, t); (t, \frac{1}{2}, 0); (0, t, \frac{1}{2})\} \quad \text{with space group} \quad Pm\bar{3}n$$

$$^+\Pi = \{(\frac{1}{4}, 0, t); (\frac{3}{4}, \frac{1}{2}, t); (t, \frac{1}{4}, 0); (t, \frac{3}{4}, \frac{1}{2}); (0, t, \frac{1}{2}); (\frac{1}{2}, t, \frac{3}{4})\} \quad \text{with space group} \quad I4_132$$

and the four sets Γ, $^+\Sigma$, $^+\Omega$, and $\Sigma^\star$ in $\langle 111 \rangle$ directions have the following parametric forms of lines. Note that $\bar{t}$ means $-t$ in crystallographic notation.

$$\Gamma = \{(t, t, t); (\bar{t}, \frac{1}{2} - t, t); (\frac{1}{2} + t, \bar{t}, t); (\frac{1}{2} - t, \frac{1}{2} + t, t)\} \quad \text{with space group} \quad Ia\bar{3}d$$

$$^+\Sigma = \{(\frac{1}{3} + t, \frac{2}{3} + t, t); (\frac{2}{3} - t, \frac{5}{6} - t, t); (\frac{1}{6} + t, \frac{2}{3} - t, t); (\frac{5}{6} - t, \frac{5}{6} + t, t)\}$$

$$\Omega^+ = \{(\frac{1}{3} + t, \frac{2}{3} + t, t); (\frac{2}{3} - t, \frac{1}{3} - t, t); (\frac{2}{3} + t, \frac{2}{3} - t, t); (\frac{1}{3} - t, \frac{1}{3} + t, t)\}$$

$$\Sigma^\star = \{(\frac{2}{3} + t, \frac{1}{3} + t, t); (\frac{1}{3} - t, \frac{1}{6} - t, t); (\frac{5}{6} + t, \frac{1}{3} - t, t); (\frac{1}{6} - t, \frac{1}{6} + t, t)\}$$

$^+\Sigma$, Ω^+, and $\Sigma^\star$ have space groups $I4_132$, $I432$, and $Ia\bar{3}d$.

From Section 2.5, these six models become links in the three-torus. These examples form a simple, but non-trivial set for us to build up techniques for computing invariants by hand. Therefore, we will deal with these six invariant cylinder packings during this thesis.

2.7 Related work

2.7.1 Primitive cells and Optimal Calculations

In Section 2.3, we mentioned that textile patterns are 2-D periodic patterns which can be shown in a 2-torus diagram. Some numerical invariants of these 2-D structures such as crossing numbers (double points), the number of components, linking number (for 2-structures, linking number is the absolute value of the sum of all crossing signs in different components [Grishanov et al., 2009]), and periodicity vectors are computed in Grishanov et al. [2009]. As we can see in Figure (2.17), any lattice parallelogram of unit area or its translated copy can be taken as a unit cell. Such a parallelogram contains the same number of crossings as the original unit square. Therefore, there exist infinitely many choices of fundamental domain. These fundamental domains are precisely primitive unit cell in definition 4.

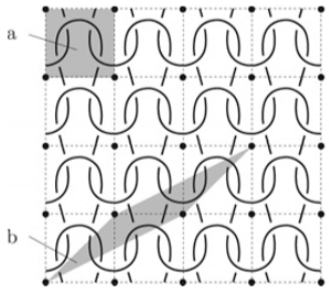

Figure 2.17: Two equivalent primitive unit cells [Grishanov et al., 2009]

For 2-D patterns in textile industry, the traditional definition of the unit cell in textile technology is the periodic manner of operation of textile machinery. And also for 3-D patterns crystallographers sometimes use the most convenient cell to represent a crystal. However, in topological terms, the unit cell must show the minimum of quantities related to that pattern (for example, crossing numbers) Grishanov et al. [2009]. In fact, we seek a region that will give the optimal computation.The primitive cell (or fundamental domain) is the only region able to answer this desire, as it has the smallest area or volume that can recreate the whole pattern under the lattice translations (see and compare the area of two unit cells in Figure (2.15)).

In Figure (2.18), there is an example of a doubly periodic pattern, where two different domains of the pattern give us two different crossing numbers. The minimum crossing number discriminates this kind of pattern [Grishanov et al., 2009].

Therefore, we are only looking for primitive domains to compute invariants but we know there is an infinite choice of primitive cells. For doubly periodic structures, some numerical invariants are independent of these choices, including crossing numbers, linking numbers, and the number of components in the compactified unit cell [Grishanov et al., 2009]. The equivalence of torus diagrams of 2-structures should be considered up to torus twists, or in other words, all primitive unit cells are equivalent

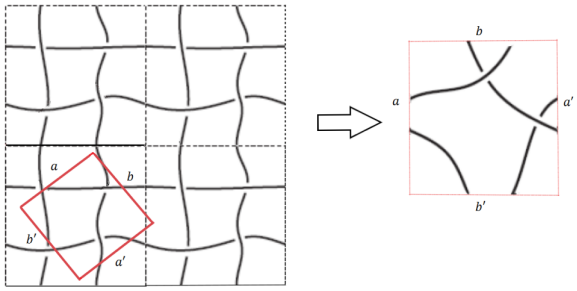

Figure 2.18: Two different cells for plain weave with unequal crossing numbers

up to linear transformations of the plane that map the integer lattice $\mathbb{Z}_2$ into itself [Grishanov et al., 2009].

In this regard, one important question that we need to address before our computations is showing if the fundamental group of the complement of 3-periodic structures is independent of choice of primitive unit cells. We will show this in Chapter 3.

In our work, except for $\Pi^\star$ which has the space group $Pm\bar{3}n$, [Hahn et al., 1983] with the primitive cubic unit cell in Table 2.1, other structures in Figure (1.1) have description of symmetry per body-centered cubic unit cell (BC), where $a = b = c$ (the length of edges of the unit cell are ll equal) and with all angles 90° (angle between edges). One choice of primitive cell of BC structures is primitive Rhombohedral unit cell (presented in Hahn et al. [1983]), where $a_1 = a_2 = a_3$ and with angles 120°. Therefore, before computing the fundamental group of the complementary space for these packings, we need to make a choice of basis vectors in $\mathbb{R}^3$ where we can build this Rhombohedral unit cell for optimal computations.

If the conventional unit cell (Body-centered unit cell) has this basis vectors,

$$\{a = (1,0,0); b = (0,1,0); c = (0,0,1)\}$$

one option of basis vectors for primitive unit cell (Rhombohedral unit cell) will be,

$$\{a_1 = (-\frac{1}{2}, -\frac{1}{2}, -\frac{1}{2}); a_2 = (-\frac{1}{2}, \frac{1}{2}, \frac{1}{2}); a_3 = (\frac{1}{2}, \frac{1}{2}, -\frac{1}{2})\}$$

This built unit cell with basis vectors, which is displayed in Figure (2.19), will be shown as a pink unit cell for each rod packing in some of the figures in this study.

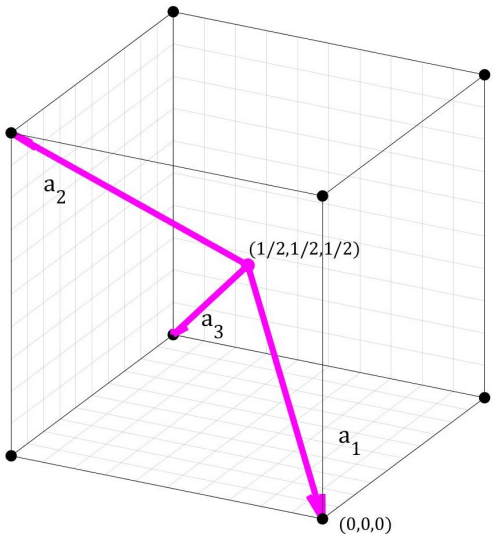

Figure 2.19: Basis vectors for the rhombohedral primitive unit cell for the non-primitive cubic unit cell

Symbol	Axes	Sp.gr	[uvw]	Origin	μ
Π^*	3-way	$Pm\bar{3}n$	[100]	0,0,0	3
${}^{+}\Pi$	3-way	$I4_132$	[100]	0.2,0,0.2	3
Γ	4-way	$Ia\bar{3}d$	[111]	0,0,0	4
${}^{+}\Sigma$	4-way	$I4_132$	[111]	0,0,0	4
${}^{+}\Omega$	4-way	$I432$	[111]	0,0,0	4
Σ^*	4-way	$Ia\bar{3}d$	[111]	0,0,0	8

Table 2.2: Six invariant cylinder packings [O'Keeffe et al., 2001] with number of different directions of axes, space group, direction of axes in the conventional unit cell, and the origin of primitive unit cell for each structure. Sometimes we need to shift the origin to get the whole structure inside this unit cell. μ is the number of components of each structure in the primitive unit cell which can show a discrimination between some of structures. We show these numbers in Chapter 3.

2.7.2 Isotopies by PB SONO algorithm

From Section 2.3, distinct knots or links are structures that cannot be deformed to one another without allowing their arcs to pass through each other, and their complementary volumes are not homeomorphic. Similarly, inequivalent cylinder packings can be recognised by their non-homeomorphic complementary spaces.

Evans et al. [2013] presented a physical simulation which adapts a numerical implementation called PB-SONO algorithm for finite knots and periodic branched structures (Shrink- On-No-Overlaps or SONO algorithm Pierański [1998] is specifically for finite knots, see Figure (2.20)). The corresponding algorithm finds the local minimum energy conformation of these structures by minimizing the ropelength D/L (L is the length, and D is the diameter of the rope that traces out the thickened arc of a knot).

This procedure requires fattening each arc during which the ratio of D to unit cell size must be considered fixed, then slightly shrink D which allows us to straighten the corresponding arc. During this procedure, arcs cannot pass through each other; so we can do this tension process multiple times. Then we make sure the distinct parts of the structure do not overlap and if for example two nodes are overlapping, we displace them away from each other symmetrically, and finally we should inflate the diameter to it's original size. Then one needs to check all conformations for all the unit cell size and shape, and take one of them as the ideal conformation with the least ropelength among all choices of unit cells [Evans et al., 2015].

By this algorithm, a taxonomy of 3-periodic weavings was presented in Evans et al. [2013]. This work has shown all parallel and layered rod packings in Table 2.1 converge to a structure with one rod per unit cell when one is allowed to change the unit cell during this process. In this sense, they are physically equivalent (ambient isotopic), and this equivalency means they have converged to a structure with one rod per unit cell within a specified tolerance.

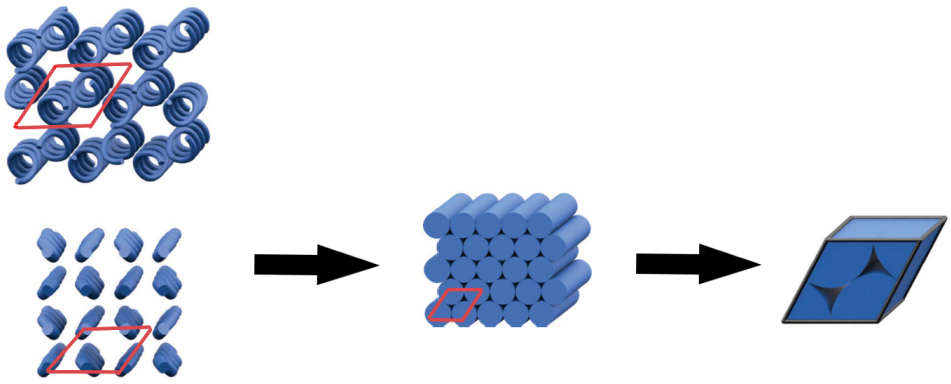

Figure 2.20: The tight embedding of parallel rod packings with 2 rods and 1 rod per unit cell, which converge to a primitive unit cell with single rod on tightening process [Evans et al., 2013]

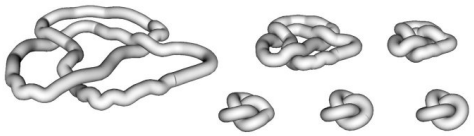

Figure 2.21: The SONO algorithm for trefoil [Pierański, 1998]

Figure (2.20) shows two parallel rod packings (honeycomb packing and square packing) which are isotopic Evans et al. [2013]. On the process of PB-SONO algorithm, both patterns in Figure (2.20) form the two-dimensional hexagonal conformation by straightening, rearrangement of cylinders, and also getting tightened embedding per unit cell, which one of them actually gets a primitive unit cell after this procedure. Similarly by using this physical algorithm, layers of cylinders form just a single rod per primitive cell by rotation of alternate layer of rods to get parallel rods and changing unit cell, in the processing of ideal embbeding [Evans et al., 2013].

These geometrical conformations are characteristic of the topological arrangement of these structures; so our results of inequivalency between cylinder packings are different from this. We want to determine if an isotopy exists between the six cubic invariant rod packings in the last class of Table 2.1 by using a topological invariant (fundamental group of complementary space) without any distortion of the arrangement of the structures.

2.8 Summary

In this Chapter, we explained the equivalency between two classes of cylinder packings that Evans et al. [2013] presented; we focused on the third class of Table 2.1 which includes six cubic invariant cylinder packings [O'Keeffe et al., 2001]. We also expressed that for having minimal representations, one needs to consider the fundamental domain for these patterns although this is not the convenient one (Body-centred cubic unit cell) as is typically used in crystallography. Then the independency of some numerical invariants for 2-periodic structures was mentioned.

In Chapter 3, computations of the fundamental group of the complement of cylinder packings will be described by applying Theorem 2 and 3. We will also see that these computations for 3-periodic structures are independent of choice of primitive unit cell.

Chapter 3

Computation of Fundamental Groups of Complement of rod Packings

3.1 Method

To compute the periodic structure (rod packings) groups here, two systematic tools, Wirtinger presentation and Seifert-van Kampen theorem, will be applied.

Theorem 3 (Seifert-van Kampen) *Hatcher [2001]. If $X = A \cup B$ is a topological space; A and B are open, path connected subspaces of X ; $A \cap B$ is nonempty and path-connected; and $x_0 \in A \cap B$; then $\pi_1(X, x_0)$ is the free product with amalgamation of $\pi_1(A, x_0)$ and $\pi_1(B, x_0)$, with respect to the (not necessarily injective) homomorphisms*

$$I : \pi_1(A \cap B, x_0) \to \pi_1(A, x_0)$$

and

$$J : \pi_1(A \cap B, x_0) \to \pi_1(B, x_0)$$

Given group presentations

$$\pi_1(A, x_0) =< a_1, ..., a_k | \alpha_1, ..., \alpha_l >$$
$$\pi_1(B, x_0) =< b_1, ..., b_m | \beta_1, ..., \beta_n >$$
$$\pi_1(A \cap B, x_0) =< w_1, ..., w_p | \gamma_1, ..., \gamma_q >$$

The amalgamation can be presented as

$$\pi_1(X, x_0) =< a_1, ..., a_k, b_1, ..., b_m | \alpha_1, ..., \alpha_l, \beta_1, ..., \beta_n, I(w_1)J(w_1)^{-1}, ..., I(w_p)J(w_p)^{-1} > .$$

We consider n number of axes in the built primitive unit cell (as we explained in Section 2.7.1). With respect to the Van-Kampen theorem [Hatcher, 2001], we try to divide the complement space into two path-connected subspaces.

Set $X = \mathbb{T}^3 \setminus L$, where L is a link (can be a cylinder packing in the compactified unit cell). Then define $\mathbb{T}^3 = A' \cup B'$, where A' is the union of small open neighbourhood of three "standard" 2-tori, and B' is the complement of the three "standard" 2-tori, hence an open ball. Then define $A = A' \setminus L$ and $B = B' \setminus L$. This gives us $X = A \cup B$ with $A \cap B$ an open neighbourhood of a punctured sphere in X. In fact, subspace is A' that is homeomorphic to $\mathbb{T}^3 \setminus$ ball (A' is a thickened surface of the unit cell with the periodic boundary). If there are n cylinders, their complementary space in A will have $2n$ punctures. The presentation for the fundamental group of this subspace uses the generators of the 3-torus $\{a_1, a_2, a_3\}$, the diagonal across each face, and additional loops around each puncture. Subspace B is the interior of the n cylinder axes removed. This means the fundamental group of B is a free group with n generators. However, the number and density of ${}^{+}\Sigma$, ${}^{+}\Omega$, and $\Sigma^{\star}$ is larger, and it is difficult to see how the generators of $\pi_1(A \cap B, x_o)$ map into this free group presentation of $\pi_1(B, x_0)$. Therefore, we construct a presentation for $\pi_1(B, x_0)$ that uses extra generators and relations by applying the same technique as the Wirtinger presentation in Section 2.3.1 for knots and links in $\mathbb{S}^3$. This requires a good projection of B and its axes onto a plane. For this projection we use direction $[111]$ (with respect to the primitive unit cell) for ${}^{+}\Sigma$ and ${}^{+}\Omega$, but $[101]$ for $\Sigma^{\star}$ as it has two parallel rods in the $[111]$. The intersection of these two subspaces $A \cap B$ is a sphere with n punctures($\mathbb{S}^2 \setminus \{$n points$\}$), where all relations on the intersection will be computed by some loops with anti-clock directions L_i, in which the index usually presents the color of the cylinders in this case. By this description we compute $\pi_1(A, x_0)$, $\pi_1(B, x_0)$, and $\pi_1(A \cap B, x_0)$ to find the fundamental group of the complementary space of all the structures. You can see this division of the complementary space of rod packings in Figure (3.1).

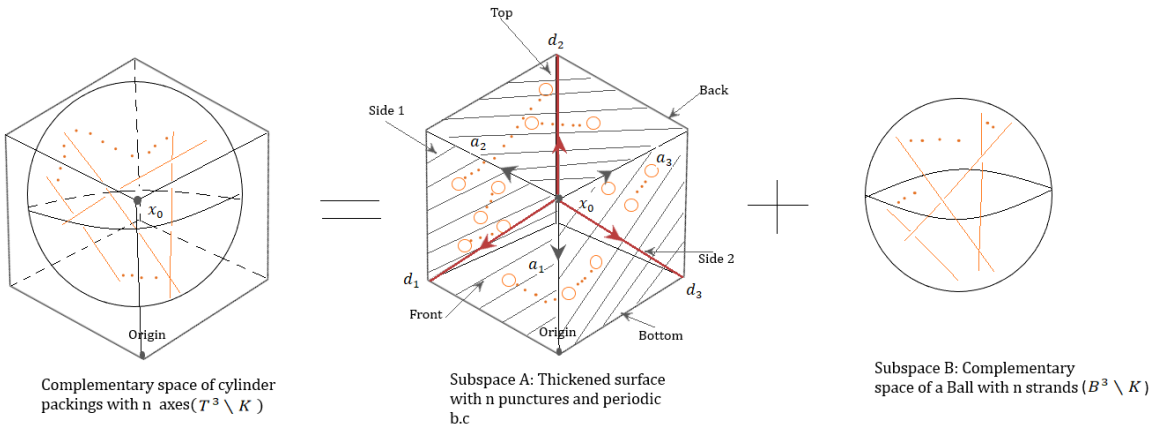

Figure 3.1: Two open, path connected subspaces for primitive cells using the idea of Seifert-van Kampen Theorem for computing the fundamental group of complementary spaces for invariant cylinder packings

First, we show the independence of these fundamental groups, for the complement of 3-periodic structures, from choices of primitive unit cell as it was mentioned

in Section 2.7.1. Suppose we have $\{a = (0,0,1), b = (1,0,0), c = (0,1,0)\}$ as the basis vectors of the original primitive unit cell P and the set $\{a' = (0,1,1), b = (1,0,0), c = (0,1,0)\}$ is the basis vectors of the sheared unit cell P' as seen in Figure (3.2). In terms of method, we explained the fundamental group of the complement of a single axis $K = (0.5, 0.5, t)$ can be computed as following steps.

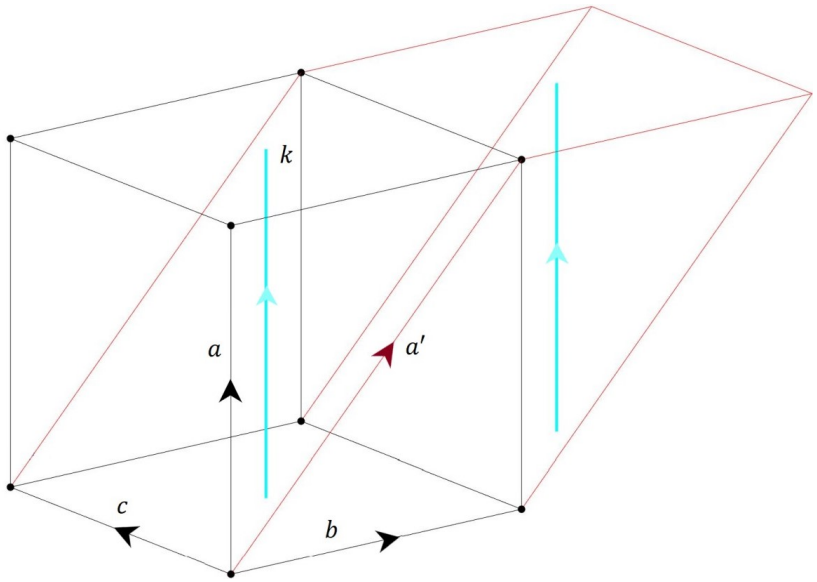

Figure 3.2: Two different primitive unit cell P with basis vectors $\{a, b, c\}$ and P' with $\{a', b, c\}$ for the structure K

In P this axis goes through the Top and Bottom faces, so the complement can deformation retract to two 2-torus which are glued along their common longitude curve a and 2 circles. Now we use Van-Kampen theorem to divide this complement space into two subspaces A and B; the first one is one torus with 1 circle and the second one is the same with another circle. Therefore, the intersection between these two subspaces is the joint point of 2 circles and one copy of $\mathbb{S}^1$ which represent that common longitude curve in both inclusion maps to A and B; therefore, we get the following group

$$\pi_1(\mathbb{T}^3 \setminus K) = f =< a, b, c | bab^{-1}a^{-1}, cac^{-1}a^{-1} >$$

The presentation of complement of the same structure in P' is slightly different. Subspace A is the $P' \setminus ball$, which deformation retracts to wedge of two additional generators α and β. These two generators can be represented by the original generators of P' with the optional direction anti clock-wise.

$$\alpha = bcb^{-1}c^{-1}$$
$$\beta = ca'^{-1}c^{-1}a'$$

The second subspace B is just a ball with two rods where one of rods is along the

Top and right side P' and the other one is along the Bottom and left side of this unit cell. Then each of these axes can be generated by a loop from basepoint like c_1 and c_2. Finally the intersection between A and B would be a sphere with four punctures so the combination of inclusion maps of each generator in intersection to the subspaces can be presented as following relations

$$ca'^{-1}c^{-1}a'c_2^{-1}, \quad a'^{-1}cbc^{-1}b^{-1}a'c_2, \quad bcb^{-1}c^{-1}c_1^{-1}, \quad ba'^{-1}ca'c^{-1}b^{-1}c_1$$

So the fundamental group is

$$\begin{aligned} g \;=\; & < a', b, c, c_1, c_2, \alpha, \beta | ca'^{-1}c^{-1}a'c_2^{-1}, \quad a'^{-1}cbc^{-1}b^{-1}a'c_2, \quad bcb^{-1}c^{-1}c_1^{-1} \\ & , \quad ba'^{-1}ca'c^{-1}b^{-1}c_1, \quad bcb^{-1}c^{-1}\alpha^{-1}, ca'^{-1}c^{-1}a'\beta^{-1} > \end{aligned}$$

But the relations of this group can be reduced by the following process. From the relations we can see

$$\begin{cases} c_1 = bcb^{-1}c^{-1} \\ c_1 = ba'^{-1}ca'c^{-1}b^{-1} \end{cases} \quad \Rightarrow \quad a'^{-1}ca'c^{-1}b^{-1}cbc^{-1}$$

$$\begin{cases} c_2 = ca'^{-1}c^{-1}a' \\ c_2 = a'^{-1}bcb^{-1}c^{-1}a' \end{cases} \quad \Rightarrow \quad a'^{-1}bcb^{-1}a'c^{-1}$$

$$\begin{cases} \alpha = bcb^{-1}c^{-1} \\ \beta = ca'^{-1}c^{-1}a' \end{cases}$$

Therefore, we can rewrite group g

$$g =< a', b, c | a'^{-1}ca'c^{-1}b^{-1}cbc^{-1}, a'^{-1}bcb^{-1}a'c^{-1}, bcb^{-1}c^{-1}, ca'^{-1}c^{-1}a' >$$

From first and last relations we can conclude $b^{-1}cbc^{-1} = 1$ and that means $bc = cb$, but this is something that can be found from the third relation, so we remove this. Again from the third relation we know $c = bcb^{-1}$, then we substitude c in the second relation, so we can get $ca' = ca'$ which trivial, so we can omit this. Now what we have in this group is

$$g =< a', b, c | bcb^{-1}c^{-1}, ca'^{-1}c^{-1}a' >$$

So there is an isomorphism $\phi : f \to g$ which $\phi(a) = c$, $\phi(b) = b$, and $\phi(c) = a'$.

Now as we know the automorphism of the three-torus is generated by $\mathbb{GL}(3, \mathbb{Z})$ [Johnson, 2011], so any arbitrary primitive unit cell can be mapped into another one by a change-of-coordinates matrix which is unimodular [Engel et al., 2004]. In other words, we are allowed to suppose two different versions of the three-torus like $\mathbb{T}^{3'} = A \cup B/L$ and $\mathbb{T}^3 = A' \cup B'/L$ where $\{A, B\}$ is a different set of subspaces for the three-torus from the set $\{A', B'\}$, but we know these two versions must be home-

omorphic by a twist. In this sense, we can claim that these groups are independent from the choice of primitive unit cells for more general examples of primitive cells.

In this regard, we can take the rhombohedral primitive unit cell as we mentioned in Section 2.7.1, and then compute the fundamental groups for the structures.

Below, we will compute all groups of the complementary space for the six invariant cylinder packings in Table 2.2.

3.2 Computations for the group of the complementary space of $\Pi^\star$

The first cylinder packing for which we compute the fundamental group of the complementary space in cubic primitive unit cell is Π^*, which is the intergrowth of ${}^{+}\Pi$ and its mirror image ${}^{-}\Pi$. The direction of the axes is $[100]$ with symmetry $Pm\bar{3}n$, and the axes are:

$$\{(0.5, 0, t); (t, 0.5, 0); (0, t, 0.5)\}$$

The unit cell in Figure (3.3) is already primitive with origin $(0, 0, 0)$. This cube has the axes on its faces and we adjust the origin to $(-0.2, -0.2, -0.2)$ so that the axes are interior to this primitive cubic unit cell. The anti-clock wise direction is selected for all the loops. This structure has nine different generators for the complementary space with 3 components and 12 relations between these 9 generators.

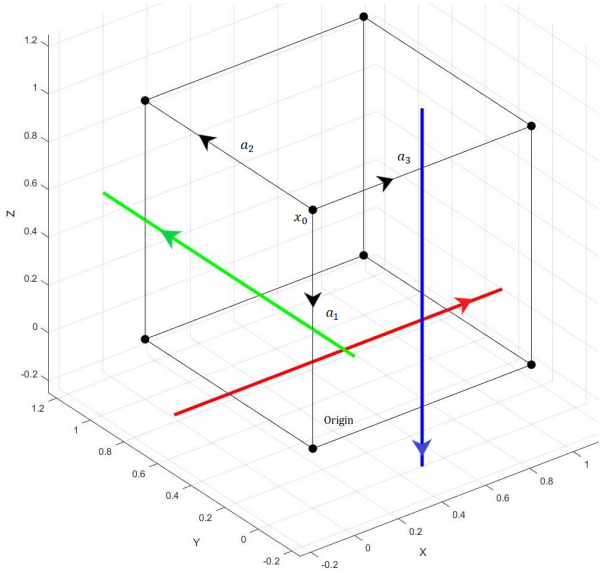

Figure 3.3: Cylinder packing Π^* in cubic primitive cell

The fundamental group of the first subspace A is three circles, (see Figure (3.4)), which can be written as the following relations:

$$\pi_1(A, x_0) =< a_1, a_2, a_3, \alpha, \beta, \gamma | \quad \alpha = a_3 a_2 a_3^{-1} a_2^{-1}, \beta = a_2 a_1 a_2^{-1} a_1^{-1}, \gamma = a_1 a_3 a_1^{-1} a_3^{-1} >$$

This group can be reduced to a group with generators a_1, a_2, and a_3, so we get a free group $< a_1, a_2, a_3 >$. The second subspace B is homeomorphic to a ball with three different untangled arcs removed, so the fundamental group of this subspace is achieved by three different loops or generators from basepoint x_0 which can track each rod independently, so that $\pi_1(B)$ is also a free group generated by three loops c_1, c_2, and c_3, see Figure (3.4).

$$\pi_1(B, x_0) =< c_1, c_2, c_3 >$$

Now the intersection of these two subspaces is homeomorphic to a spherical shell with loops L_{t_i} and $\overline{L_{t_i}}$ as the generators, where t represents the first letter of the colour of the axis. With respect to the direction, when the axis enters the cell we selected the first symbol L_{t_i}, and when it exits we used the second symbol $\overline{L_{t_i}}$. In this notation, the relations on the intersection of two subspaces A and B are; see Figure (3.5). As one can see in Figure (3.3), we cannot trace the red rod on the intersection subspace without passing over the green rod, which means the relations for homomorphism J sometimes is generated by multiple generators c_i.

$$\begin{aligned} \pi_1(A \cap B, x_0) \quad &= \quad < L_r, \overline{L_r}, L_g, \overline{L_g}, L_b, \overline{L_b} \\ &| \quad \overline{L}_b L_g \overline{L}_r L_b \overline{L}_g L_r > \end{aligned}$$

Injective homomorphism I	Injective homomorphism J
$I(L_b) =< a_3 a_2 a_3^{-1} a_2^{-1} >$	$J(L_b) =< c_2^{-1} >$
$I(\overline{L_b}) =< a_3 a_1 a_3^{-1} a_2 a_3 a_2^{-1} a_1^{-1} a_3^{-1} >$	$J(\overline{L_b}) =< c_2 >$
$I(L_r) =< a_2 a_1 a_2^{-1} a_1^{-1} >$	$J(L_r) =< c_3^{-1} c_1^{-1} c_3 >$
$I(\overline{L_r}) =< a_3 a_1 a_2 a_1^{-1} a_2^{-1} a_3^{-1} >$	$J(\overline{L_r}) =< c_2^{-1} c_1 c_2 >$
$I(L_g) =< a_1 a_3 a_1^{-1} a_3^{-1} >$	$J(L_g) =< c_3^{-1} >$
$I(\overline{L_g}) =< a_2 a_3 a_1 a_3^{-1} a_1^{-1} a_2^{-1} >$	$J(\overline{L_g}) =< c_3 >$

Table 3.1: Injective homomorphisms on the intersection of two subspaces as mentioned in Theorem 3

$I(L_b)J(L_b)^{-1} =< a_3 a_2 a_3^{-1} a_2^{-1} c_2 >$	$I(\overline{L_b})J(\overline{L_b})^{-1} =< a_3 a_1 a_3^{-1} a_2 a_3 a_2^{-1} a_1^{-1} a_3^{-1} c_2^{-1} >$
$I(L_r)J(L_r)^{-1} =< a_2 a_1 a_2^{-1} a_1^{-1} c_3^{-1} c_1 c_3 >$	$I(\overline{L_r})J(\overline{L_r})^{-1} =< a_3 a_1 a_2 a_1^{-1} a_2^{-1} a_3^{-1} c_2^{-1} c_1^{-1} c_2 >$
$I(L_g)J(L_g)^{-1} =< a_1 a_3 a_1^{-1} a_3^{-1} c_3 >$	$I(\overline{L_g})J(\overline{L_g})^{-1} =< a_2 a_3 a_1 a_3^{-1} a_1^{-1} a_2^{-1} c_3^{-1} >$

Table 3.2: Relations on intersection of subspaces $A\&B$ for $\Pi^\star$

Therefore, the final presentation of the complementary space for this cylinder packing will be as following, where you can see the relations in Table 3.1 and 3.2

$$\begin{aligned}\pi_1(\mathbb{T}^3 \setminus \Pi^\star) &= < a_1, a_2, a_3, c_1, c_2, c_3 | a_3 a_2 a_3^{-1} a_2^{-1} c_2, a_3 a_1 a_3^{-1} a_2 a_3 a_2^{-1} a_1^{-1} a_3^{-1} c_2^{-1} \\ &, \quad a_1 a_3 a_1^{-1} a_3^{-1} c_3, a_2 a_3 a_1 a_3^{-1} a_1^{-1} a_2^{-1} c_3^{-1}, a_2 a_1 a_2^{-1} a_1^{-1} c_3^{-1} c_1 c_3 \\ &, \quad a_3 a_1 a_2 a_1^{-1} a_2^{-1} a_3^{-1} c_2^{-1} c_1^{-1} c_2 > . \end{aligned} \tag{3.1}$$

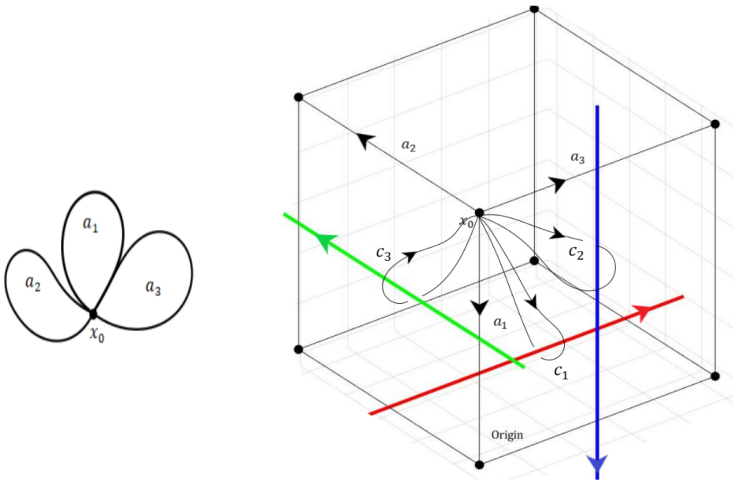

Figure 3.4: From left, subspace A, then subspace B with generators c_1, c_2, and $c_3$for cylinder packing $\Pi^\star$. Each loop in the first figure from left is related to the original generators for the three-torus. In the second subspace C_i's are the generators for the loops around the center from the basepoint.

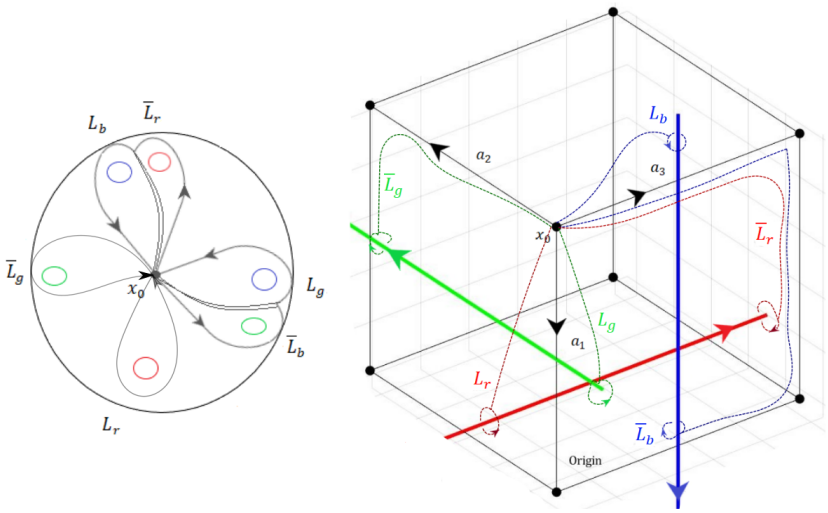

Figure 3.5: From left, subspace $A \cap B$ for the complement of cylinder packing $\Pi^{\star}$ which are loops with anti-clock wise directions. On the right, one can see the trace for each loop on the thin layer of the shell inside the unit cell

3.3 Computations for the group of the complementary space of ${}^{+}\Pi$

The second invariant cylinder packing is ${}^{+}\Pi$ with again direction$[100]$, symmetry $I4_132$, and axes generated by all integer translation copies of:

$$\{(0.25, 0, t); (0.75, 0.5, t); (t, 0.25, 0); (t, 0.75, 0.5); (0, t, 0.25); (0.5, t, 0.75)\}$$

The standard unit cell of this cylinder packing is a cubic body-centered cell. Therefore, we build the primitive unit cell generated by three independent basis vectors $\{a_1 = (-0.5, -0.5, -0.5); a_2 = (-0.5, 0.5, 0.5); a_3 = (0.5, 0.5, -0.5)\}$ instead (see the primitive rhombohedral cell in Figure(3.6)). In this primitive cell, the following axes are the ones that pass through the primitive cell as drawn.

$$\{(0.25, 1, t); (-0.25, 0.5, t); (t, 0.25, 0); (t, 0.75, 0.5); (0, t, 0.25); (0.5, t, -0.25)\}$$

To determine subspace A and its deformation retraction, one needs to find the intersection point of each axis with the faces of the primitive unit cell. If we look at Figure (3.6) with the origin at the lower front as drawn, this primitive unit cell has the following faces

1. Top Face $= \{x + z = 1 | \quad 0 \leqslant x \leqslant 1; 0.5 \leqslant y \leqslant 1.5; 0 \leqslant z \leqslant 1\}$
2. Front Face $= \{z - y = 0 | \quad -0.5 \leqslant x \leqslant 0.5; 0 \leqslant y \leqslant 1; 0 \leqslant z \leqslant 1\}$
3. Bottom Face $= \{x + z = 0 | \quad -0.5 \leqslant x \leqslant 0.5; 0 \leqslant y \leqslant 1; -0.5 \leqslant z \leqslant 0.5\}$

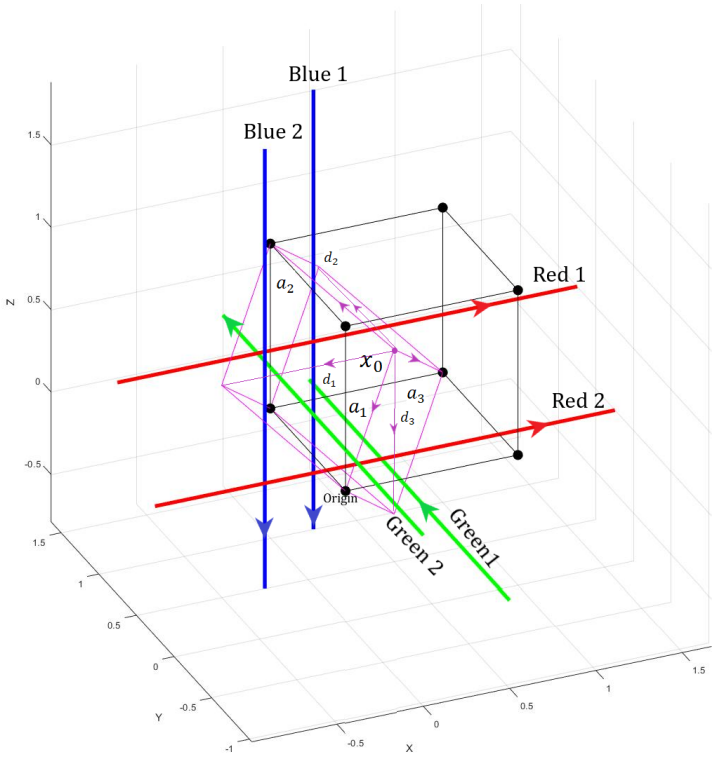

Figure 3.6: Cylinder packing $^{+}\Pi$ in cubic primitive cell

4. Back Face $= \{-y+z=-1| \quad 0 \leqslant x \leqslant 1; 0.5 \leqslant y \leqslant 1.5; -0.5 \leqslant z \leqslant 0.5\}$

5. Side 1 Face $= \{x-y=-1| \quad -0.5 \leqslant x \leqslant 0.5; 0.5 \leqslant y \leqslant 1.5; 0 \leqslant z \leqslant 1\}$

6. Side 2 Face $= \{-x+y=0| \quad 0 \leqslant x \leqslant 1; 0 \leqslant y \leqslant 1; -0.5 \leqslant z \leqslant 1\}$

By using the equations of the rod axes and faces, we can easily find the intersection points between axes and faces. We must consider the interior axes in the primitive unit cell. In this regard, these equations and the intervals help us to find the position of each rod.

For example Blue 1 in Figure (3.6) intersects the Top and Back faces. Blue 2 goes through the Front face and exits through the Bottom face. Red 1 comes from the face Side 1 (on the right) and outs from the Top face. The second Red rod comes from the Bottom face and quits Side 2 (on the left). Green 1 comes from the Side 2 face and outs the Back Face, and the second green rod goes through the Front face, outing the Side 1 face.

Therefore, the subspace A of the complementary space of this rod packing, will have two punctures in each of its faces, and so deformation retracts to six circles in figure (3.7). In this case, each circle can be presented by a generator α_i,β_i, and γ_i, but these again can be expressed by some relations with the original generators of the cell a_i and d_i, where d_i are the diagonals of each face applied as the auxiliary vectors

to have an easier presentation for circles.

$$\begin{aligned}\pi_1(A,x_0) &= < a_i,d_i,\alpha_i,\beta_i,\gamma_i|\alpha_1 = d_2a_3^{-1}a_2^{-1},\alpha_2 = a_2a_1d_1^{-1},\beta_1 = a_3a_2d_2^{-1}\\ &, \quad \beta_2 = a_1a_3d_3^{-1},\gamma_1 = d_1a_2^{-1}a_1^{-1},\gamma_2 = d_3a_1^{-1}a_3^{-1} >\end{aligned}$$

But because these generators $\{\alpha_i,\beta_i,\gamma_i\}$ are redundant, we can rewrite the group.

$$\pi_1(A,x_0) =< a_1,a_2,a_3,d_1,d_2,d_3 >$$

The second subspace of the complementary space is again a ball with six different cylinder axes removed, so the group has six generators $\{c_1,c_2,c_3,c_4,c_5,c_6\}$ as shown in Figure(3.7).

$$\pi_1(B,x_0) =< c_1,c_2,\ldots,c_6 >$$

The relations for ${}^{+}\Pi$ on the $A \cap B$ are as below, see Figure (3.8):

$$\begin{aligned}\pi_1(A\cap B,x_0) &= < L_{r_1},L_{r_2},\overline{L_{r_1}},\overline{L_{r_2}},L_{g_1},L_{g_2},\overline{L_{g_1}},\overline{L_{g_2}},L_{b_1},L_{b_2},\overline{L_{b_1}},\overline{L_{b_2}}\\ &| \quad \overline{L}_{b_2}\overline{L}_{b_1}L_{g_2}L_{g_1}\overline{L}_{r_2}\overline{L}_{r_1}L_{b_1}L_{b_2}\overline{L}_{y_1}\overline{L}_{y_2}L_{r_1}L_{r_2} >\end{aligned}$$

Injective homomorphism I	Injective homomorphism J
$I(L_{b_1}) =< d_2a_3^{-1}a_2^{-1} >$	$J(L_{b_1}) =< c_5^{-1}c_1^{-1}c_5 >$
$I(\overline{L_{b_1}}) =< a_3a_1a_2d_1^{-1}a_3^{-1} >$	$J(\overline{L_{b_1}}) =< c_1 >$
$I(L_{b_2}) =< a_2a_1d_1^{-1} >$	$J(L_{b_2}) =< c_6^{-1} >$
$I(\overline{L_{b_2}}) =< d_1a_3d_2^{-1}a_2d_1^{-1} >$	$J(\overline{L_{b_2}}) =< c_6 >$
$I(L_{r_1}) =< a_2d_3a_3^{-1}a_1^{-1}a_2^{-1} >$	$J(L_{r_1}) =< c_5^{-1} >$
$I(\overline{L_{r_1}}) =< a_3a_2d_2^{-1} >$	$J(\overline{L_{r_1}}) =< c_5 >$
$I(L_{r_2}) =< a_1d_2a_2^{-1}a_3^{-1}a_1^{-1} >$	$J(L_{r_2}) =< c_2^{-1} >$
$I(\overline{L_{r_2}}) =< a_1a_3d_3^{-1} >$	$J(\overline{L_{r_2}}) =< c_2 >$
$I(L_{g_1}) =< d_3a_1^{-1}a_3^{-1} >$	$J(L_{g_1}) =< c_3^{-1} >$
$I(\overline{L_{g_1}}) =< a_3d_1a_1^{-1}a_2^{-1}a_3^{-1} >$	$J(\overline{L_{g_1}}) =< c_3 >$
$I(L_{g_2}) =< d_1a_2^{-1}a_1^{-1} >$	$J(L_{g_2}) =< c_4^{-1} >$
$I(\overline{L_{g_2}}) =< a_2a_3a_1d_3^{-1}a_2^{-1} >$	$J(\overline{L_{g_2}}) =< c_4 >$

Table 3.3: Injective homomorphisms on the intersection of two subspaces with respect to the notations from Theorem 3

Finally, all relations and generators for the complementary space of ${}^{+}\Pi$ are achieved (see Table 3.3, and 3.4). Therefore, the complementary space can be rep-

$I(L_{b_1})J(L_{b_1})^{-1} =< d_2a_3^{-1}a_2^{-1}c_5^{-1}c_1c_5 >$	$I(\overline{L_{b_1}})J(\overline{L_{b_1}})^{-1} =< a_3a_1a_2d_1^{-1}a_3^{-1}c_1^{-1} >$
$I(L_{b_2})J(L_{b_2})^{-1} =< a_2a_1d_1^{-1}c_6 >$	$I(\overline{L_{b_2}})J(\overline{L_{b_2}})^{-1} =< d_1a_3d_2^{-1}a_2d_1^{-1}c_6^{-1} >$
$I(L_{r_1})J(L_{r_1})^{-1} =< a_2d_3a_3^{-1}a_1^{-1}a_2^{-1}c_5 >$	$I(\overline{L_{r_1}})J(\overline{L_{r_1}})^{-1} =< a_3a_2d_2^{-1}c_5^{-1} >$
$I(L_{r_2})J(L_{r_2})^{-1} =< a_1d_2a_2^{-1}a_3^{-1}a_1^{-1}c_2 >$	$I(\overline{L_{r_2}})J(\overline{L_{r_2}})^{-1} =< a_1a_3d_3^{-1}c_2^{-1} >$
$I(L_{g_1})J(L_{g_1})^{-1} =< d_3a_1^{-1}a_3^{-1}c_3 >$	$I(\overline{L_{g_1}})J(\overline{L_{g_1}})^{-1} =< a_3d_1a_1^{-1}a_2^{-1}a_3^{-1}c_3^{-1} >$
$I(L_{g_2})J(L_{g_2})^{-1} =< d_1a_2^{-1}a_1^{-1}c_4 >$	$I(\overline{L_{g_2}})J(\overline{L_{g_2}})^{-1} =< a_2a_3a_1d_3^{-1}a_2^{-1}c_4^{-1} >$

Table 3.4: Relations on intersection of subspaces $A\&B$ for ${}^{+}\Pi$

resented as the following group;

$$\begin{aligned}\pi_1(\mathbb{T}^3 \setminus {}^{+}\Pi) \;=\; & < a_1, a_2, a_3, d_1, d_2, d_3, c_1, c_2, c_3, c_4, c_5, c_6 | d_2a_3^{-1}a_2^{-1}c_5^{-1}c_1c_5 \\ & , \; a_3a_1a_2d_1^{-1}a_3^{-1}c_1^{-1}, a_2a_1d_1^{-1}c_6, d_1a_3d_2^{-1}a_2d_1^{-1}c_6^{-1}, a_2d_3a_3^{-1}a_1^{-1}a_2^{-1}c_5 \\ & , \; a_3a_2d_2^{-1}c_5^{-1}, a_1d_2a_2^{-1}a_3^{-1}a_1^{-1}c_2, a_1a_3d_3^{-1}c_2^{-1}, d_3a_1^{-1}a_3^{-1}c_3 \\ & , \; a_3d_1a_1^{-1}a_2^{-1}a_3^{-1}c_3^{-1}, d_1a_2^{-1}a_1^{-1}c_4, a_2a_3a_1d_3^{-1}a_2^{-1}c_4^{-1} > . \end{aligned} \tag{3.2}$$

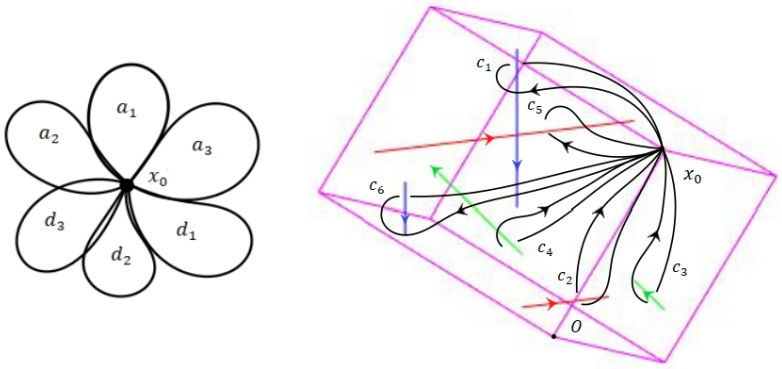

Figure 3.7: From left subspace A, then subspace B with six generators, in the primitive cell included cylinder axes removed for cylinder packing ${}^{+}\Pi$

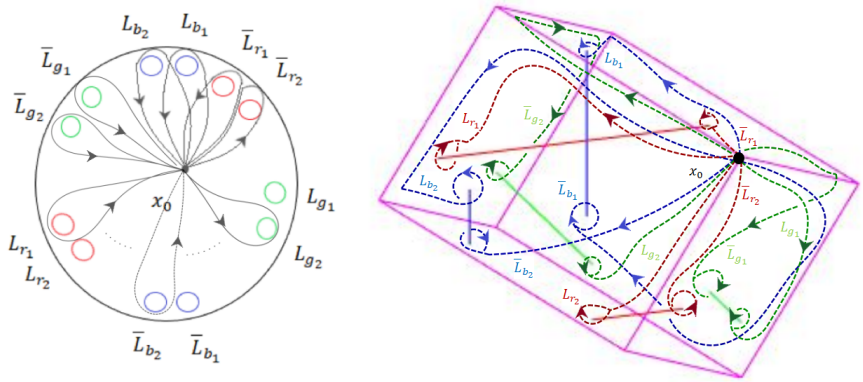

Figure 3.8: From left, the homeomorphic image (punctures can be permuted arbitrarily) for subspace $A \cap B$ which is the shell of a ball in the primitive cell and also the trace of each loop on the right with anti-clock wise direction for the complement of ${}^{+}\Pi$

3.4 Computations for the group of the complementary space of Γ

The next invariant cylinder packing is Γ with rods along the $< 111 >$ direction, symmetry $Ia\bar{3}d$, and axes as

$$\{(t,t,t);(\bar{t},0.5-t,t);(0.5+t,\bar{t},t);(0.5-t,0.5+t,t)\}$$

The original unit cell of this structure is again body-centered. We consider the same linearly-independent three basis vectors as we considered for the ${}^{+}\Pi$ for having the primitive cell but we just need to move primitive unit cell basepoint to $(0.2,0,0.2)$ in this case in order to have all axes inside the constructed primitive rhombohedral cell. Therefore, the internal axes are as the following set of axes, see Figure (3.9):

$$\{(t,t,t);(0.5-t,0.5+t,t);(t+0.5,-t,t+1) \quad ;$$
$$(t+0.5,-t+1,t+1);(t+0.5,-t+1,t);(-t,0.5-t,t+1)\}$$

Now, for subspace A of the complementary space for this structure where the deformation retracts to the wedge of the circles, we need to compute the intersection points of these axes with the faces of the constructed primitive unit cell, which are as the following faces, and again we are looking from the origin $(0.2,0,0.2)$ here.

1. Top Face $= \{x+z=\frac{7}{5}|\frac{1}{5}\leqslant x\leqslant\frac{6}{5};\frac{1}{2}\leqslant y\leqslant\frac{3}{2};\frac{1}{5}\leqslant z\leqslant\frac{6}{5}\}$
2. Front Face $= \{y-z=-\frac{4}{5}|-\frac{3}{10}\leqslant x\leqslant\frac{7}{10};0\leqslant y\leqslant 1;\frac{1}{5}\leqslant z\leqslant\frac{6}{5}\}$
3. Bottom Face $= \{x+z=\frac{2}{5}|-\frac{3}{10}\leqslant x\leqslant\frac{7}{10};0\leqslant y\leqslant 1;-\frac{3}{10}\leqslant z\leqslant\frac{7}{10}\}$
4. Back Face $= \{-y+z=-\frac{4}{5}|\frac{1}{5}\leqslant x\leqslant\frac{6}{5};\frac{1}{2}\leqslant y\leqslant\frac{3}{2};\frac{1}{5}\leqslant z\leqslant\frac{7}{10}\}$

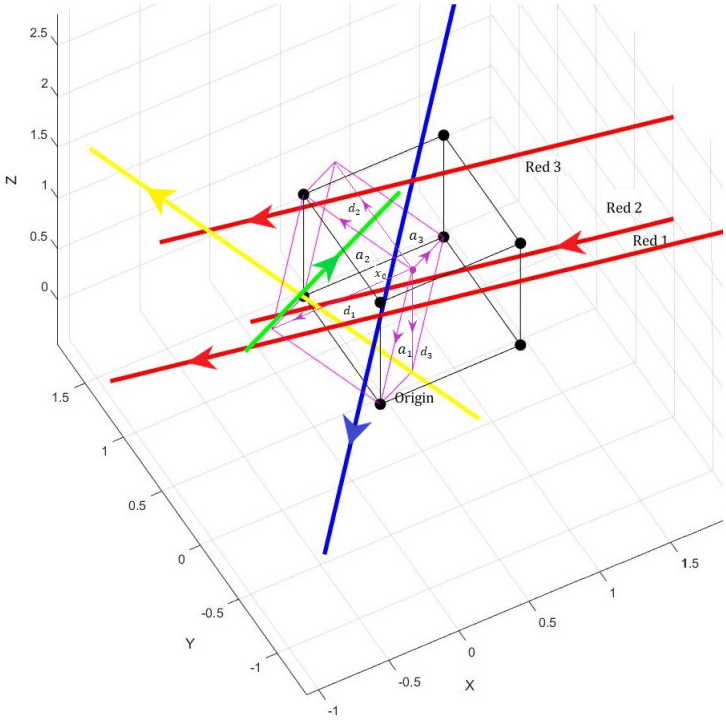

Figure 3.9: Cylinder packing Γ in rhombohedral primitive cell

5. Side1 Face (left) $= \{x - y = -\frac{4}{5} | -\frac{3}{10} \leqslant x \leqslant \frac{7}{10}; \frac{1}{2} \leqslant y \leqslant \frac{3}{2}; \frac{1}{5} \leqslant z \leqslant \frac{6}{5}\}$
6. Side2 Face $= \{-x + y = -\frac{1}{5} | \frac{1}{5} \leqslant x \leqslant \frac{6}{5}; 0 \leqslant y \leqslant 1; -\frac{3}{10} \leqslant z \leqslant \frac{6}{5}\}$

- Green rod goes from Front face to the Back face:
  - Intersection point with Back face: $(0.65, 1.15, 0.35)$
  - Intersection point with Front face:$(0.15, 0.65, 0.85)$
- Red 1 rod goes from the front face to the Bottom face:
  - Intersection point with Front face:$(0.1, 0.4, 0.6)$
  - Intersection point with Bottom face:$(-0.05, 0.55, 0.45)$
- Red 2 goes from the second side (right) face to the Back face :
  - Intersection point with Back face:$(0.6, 0.9, 0.1)$
  - Intersection point with Side 2 face:$(0.85, 0.65, 0.35)$
- Red 3 goes from the Top face to the Side 1:
  - Intersection point with Top face:$(0.45, 1.05, 0.95)$
  - Intersection point with Side 1 face:$(0.35, 1.15, 0.85)$

- Yellow rod goes from Side 2 to Side1:
  - Intersection point with Side 2 face:$(0.6, 0.4, -0.1)$
  - Intersection point with Side 1 face:$(0.1, 0.9, 0.4)$
- Blue rod goes from Top face to the Bottom face:
  - Intersection point with Bottom face:$(0.2, 0.2, 0.2)$
  - Intersection point with Top face:$(0.7, 0.7, 0.7)$

Therefore, the subspace A is a surface with 12 punctures where the deformation retracts to 6 different circles in figure (3.10), and can be presented by $\{\alpha, \gamma, \lambda, \beta_1, \beta_2, \beta_3\}$ as their generators which again could be expressed by relations with original generators a_i, and d_i of the primitive cell.

$$\pi_1(A, x_0) =< a_i, d_i, \alpha, \gamma, \lambda, \beta_i | \quad \text{relations} >$$

The relations are,

$$\alpha = a_3 a_2 d_2^{-1}$$
$$\gamma = a_2 a_1 d_1^{-1}$$
$$\lambda = d_3 a_1^{-1} a_3^{-1}$$
$$\beta_1 = d_1 a_2^{-1} a_1^{-1}$$
$$\beta_2 = a_1 a_3 d_3^{-1}$$
$$\beta_3 = d_2 a_3^{-1} a_2^{-1}$$

Then it can be reduced to a free group;

$$\pi_1(A, x_0) =< a_1, a_2, a_3, d_1, d_2, d_3 >$$

Next subspace B is the ball with removed axes. Here, we would consider six different generators for each rod where the subspace B is a free group generated by this six elements, because these rods become six different untangled arcs in this subspace.

$$\pi_1(B, x_0) =< c_1, c_2, c_3, c_4, c_5, c_6 >$$

The relations on the intersection of these two subspaces will be expressed by the same symbols for the invariant cylinder packing ${}^{+}\Pi$.

$$\begin{aligned} \pi_1(A \cap B, x_0) \quad = \quad & < L_{r_1}, L_{r_2}, L_{r_3}, \overline{L_{r_1}}, \overline{L_{r_2}}, \overline{L_{r_3}}, L_y, \overline{L_y}, L_g, \overline{L_g}, L_b, \overline{L_b}, \\ | \quad & \overline{L_b} L_{r_1} L_{r_2} L_y L_{r_3} L_b \overline{L_g} \overline{L_{r_2}} \overline{L_{r_3}} \overline{L_y} \overline{L_{r_1}} L_g > \end{aligned}$$

Now we have identified 18 generators with 18 relations (also see Tables 3.5, and 3.6) and between them for the complementary space of Γ (The injective homeomor-

Injective homomorphism I	Injective homomorphism J
$I(L_b) =< a_3a_2d_2^{-1} >$	$J(L_b) =< c_2^{-1} >$
$I(\overline{L_b}) =< a_1d_2a_2^{-1}a_3^{-1}a_1^{-1} >$	$J(\overline{L_b}) =< c_2 >$
$I(L_y) < a_1a_3d_3^{-1} >$	$J(L_y) =< c_3^{-1} >$
$I(\overline{L_y}) =< a_2d_3a_3^{-1}a_1^{-1}a_2^{-1} >$	$J(\overline{L_y}) =< c_5^{-1}c_2c_3c_2^{-1}c_5 >$
$I(L_{r_1}) =< d_1a_2^{-1}a_1^{-1} >$	$J(L_{r_1}) =< c_1^{-1} >$
$I(\overline{L_{r_1}}) =< a_1a_2a_3d_2^{-1}a_1^{-1} >$	$J(\overline{L_{r_1}}) =< c_1 >$
$I(L_{r_2}) =< d_3a_1^{-1}a_3^{-1} >$	$J(L_{r_2}) =< c_4^{-1} >$
$I(\overline{L_{r_2}}) =< a_3a_1a_2d_1^{-1}a_3^{-1} >$	$J(\overline{L_{r_2}}) =< c_4 >$
$I(L_{r_3}) =< d_2a_3^{-1}a_2^{-1} >$	$J(L_{r_3}) =< c_6^{-1} >$
$I(\overline{L_{r_3}}) =< a_2a_3a_1d_3^{-1}a_2^{-1} >$	$J(\overline{L_{r_3}}) =< c_6 >$
$I(L_g) =< a_2a_1d_1^{-1} >$	$J(L_g) =< c_5^{-1} >$
$I(\overline{L_g}) =< a_3d_1a_1^{-1}a_2^{-1}a_3^{-1} >$	$J(\overline{L_g}) =< c_2^{-1}c_5c_2 >$

Table 3.5: Injective homomorphisms on the intersection of two subspaces as mentioned in Theorem 3

$I(L_b)J(L_b)^{-1} =< a_3a_2d_2^{-1}c_2 >$	$I(\overline{L_b})J(\overline{L_b})^{-1} =< a_1d_2a_2^{-1}a_3^{-1}a_1^{-1}c_2^{-1} >$
$I(L_y)J(L_y)^{-1} =< a_1a_3d_3^{-1}c_3 >$	$I(\overline{L_y})J(\overline{L_y})^{-1} =< a_2d_3a_3^{-1}a_1^{-1}a_2^{-1}c_5^{-1}c_2c_3^{-1}c_2^{-1}c_5 >$
$I(L_{r_1})J(L_{r_1})^{-1} =< d_1a_2^{-1}a_1^{-1}c_1 >$	$I(\overline{L_{r_1}})J(\overline{L_{r_1}})^{-1} =< a_1a_2a_3d_2^{-1}a_1^{-1}c_1^{-1} >$
$I(L_{r_2})J(L_{r_2})^{-1} =< d_3a_1^{-1}a_3^{-1}c_4 >$	$I(\overline{L_{r_2}})J(\overline{L_{r_2}})^{-1} =< a_3a_1a_2d_1^{-1}a_3^{-1}c_4^{-1} >$
$I(L_{r_3})J(L_{r_3})^{-1} =< d_2a_3^{-1}a_2^{-1}c_6 >$	$I(\overline{L_{r_3}})J(\overline{L_{r_3}})^{-1} =< a_2a_3a_1d_3^{-1}a_2^{-1}c_6^{-1} >$
$I(L_g)J(L_g)^{-1} =< a_2a_1d_1^{-1}c_5 >$	$I(\overline{L_g})J(\overline{L_g})^{-1} =< a_3d_1a_1^{-1}a_2^{-1}a_3^{-1}c_2^{-1}c_5^{-1}c_2 >$

Table 3.6: Relations on intersection of subspaces $A\&B$ for Γ

phism $J(\overline{L_y})$ needs the conjugacies with c_2 and c_5, because of the choices of inclusion with $I(\overline{L_y})$), which can be written as following:

$$\begin{aligned}\pi_1(\mathbb{T}^3 \setminus \Gamma) \;=\; & < a_1, a_2, a_3, d_1, d_2, d_3, c_1, c_2, c_3, c_4, ..., c_6 | \quad a_3a_2d_2^{-1}c_2, a_1d_2a_2^{-1}a_3^{-1}a_1^{-1}c_2^{-1} \\ & , \; a_1a_3d_3^{-1}c_3, a_2d_3a_3^{-1}a_1^{-1}a_2^{-1}c_5^{-1}c_2c_3^{-1}c_2^{-1}c_5, d_1a_2^{-1}a_1^{-1}c_1, a_1a_2a_3d_2^{-1}a_1^{-1}c_1^{-1} \\ & , \; d_3a_1^{-1}a_3^{-1}c_4, a_3a_1a_2d_1^{-1}a_3^{-1}c_4^{-1}, d_2a_3^{-1}a_2^{-1}c_6, a_2a_3a_1d_3^{-1}a_2^{-1}c_6^{-1}, a_2a_1d_1^{-1}c_5 \\ & , \; a_3d_1a_1^{-1}a_2^{-1}a_3^{-1}c_2^{-1}c_5^{-1}c_2 > . \end{aligned} \tag{3.3}$$

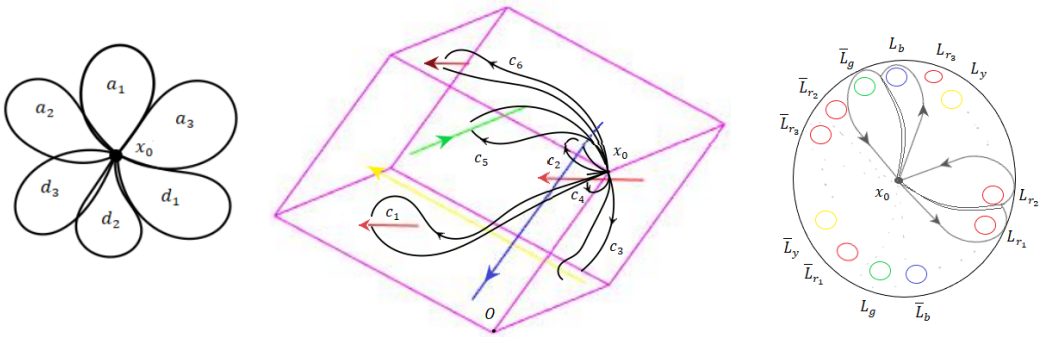

Figure 3.10: From left subspace A, B with six generators, and $A \cap B$ which is the shell of a ball in the primitive cell included cylinder axes removed for cylinder packing Γ

3.5 Computations for the group of the complementary space of ${}^{+}\Sigma$

The fourth invariant cylinder packing is ${}^{+}\Sigma$ with direction [111], symmetry $I4_132$, and axes as:

$$\{(\frac{1}{3}+t,\frac{2}{3}+t,t);(\frac{2}{3}-t,\frac{5}{6}-t,t);(\frac{1}{6}+t,\frac{2}{3}-t,t);(\frac{5}{3}-t,\frac{5}{6}+t,t)\}$$

The unit cell is similarly non-primitive here, so we will again define our common primitive rhombohedral unit cell for this cylinder packing. As it is clear in figure(3.11), the internal axes for this primitive cell will be

$$\begin{aligned}\{\quad & (\frac{1}{3}+t,\frac{2}{3}+t,t);(\frac{2}{3}-t,\frac{5}{6}-t,t);(\frac{1}{6}+t,\frac{2}{3}-t,t+1)\\ ;\quad & (\frac{1}{6}+t,\frac{5}{3}-t,t);(\frac{1}{6}+t,\frac{2}{3}-t,t);(\frac{5}{6}-t,\frac{5}{6}+t,t)\}\end{aligned}$$

- Green rod goes from Front face to Back face:
  - Intersection point with Front face;$(\frac{1}{4},\frac{5}{12},\frac{5}{12})$
  - Intersection point with Back face;$(\frac{3}{4},\frac{11}{12},-\frac{1}{12})$
- Red 1 rod goes from Top face to Back face:
  - Intersection with Top face:$(\frac{7}{12},\frac{5}{4},\frac{5}{12})$
  - Intersection with Back face:$(\frac{1}{2},\frac{4}{3},\frac{1}{3})$
- Red 2 goes Front face to the Side 1(left) face:
  - Intersection with Front face;$(0,\frac{5}{6},\frac{5}{6})$

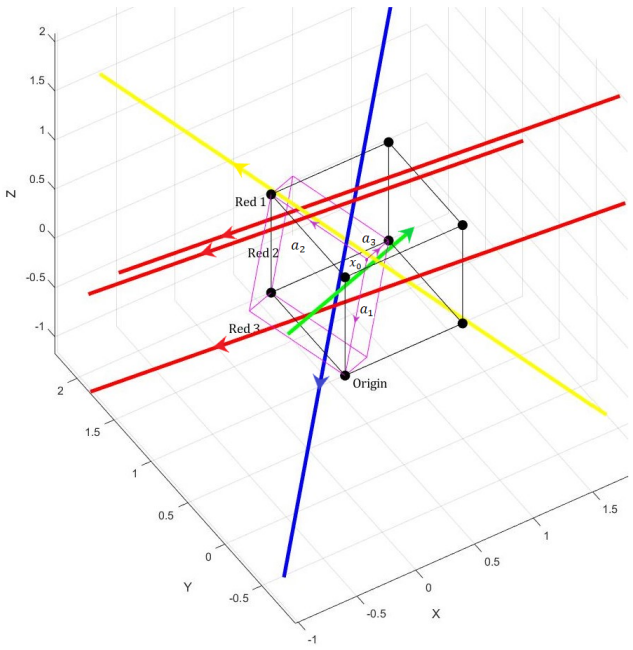

Figure 3.11: Cylinder packing $^{+}\Sigma$ in rhombohedral primitive cell

  - Intersection point with Side 1 face;$(-\frac{1}{12}, \frac{11}{12}, \frac{3}{4})$

- Red 3 goes from Side 2 face to the Bottom face:
  - Intersection with Side2 face:$(\frac{5}{12}, \frac{5}{12}, \frac{1}{4})$
  - Intersection with Bottom face:$(\frac{1}{12}, \frac{3}{4}, -\frac{1}{12})$

- Blue rod goes from Top face to the Bottom face;
  - Intersection with Top face:$(\frac{2}{3}, 1, \frac{1}{3})$
  - Intersection with the Bottom face:$(\frac{1}{6}, \frac{1}{2}, -\frac{1}{6})$

- Yellow rod goes from Side 2 to Side 1 face:
  - Intersection with the second side is:$(\frac{5}{6}, \frac{5}{6}, 0)$
  - Intersection with the first side from left:$(\frac{1}{3}, \frac{4}{3}, \frac{1}{2})$

Therefore, the subspace A of the complementary space for $^{+}\Sigma$ in the pink primitive cell in Figure (3.11) will have 2 punctures in each face, and deformation retracts to 6 generators of the cell with the three-torus structure, as shown in Figure (3.12). Similar to other structures, we can express the generators of these circles by the relations between the original generators of the unit cell $\{a_1 = (-\frac{1}{2}, -\frac{1}{2}, -\frac{1}{2}); a_2 = (-\frac{1}{2}, \frac{1}{2}, \frac{1}{2}); a_3 = (\frac{1}{2}, \frac{1}{2}, -\frac{1}{2})\}$ and diagonals $\{d_1 = (-1, 0, 0); d_2 = (-1, 0, 1); d_3 =$

$(0,0,-1)\}$. Therefore, we will have the following generators and relations for subspace A:

$$\pi_1(A,x_0) =< a_1,a_2,a_3,d_1,d_2,d_3,\alpha,\beta_1,\beta_2,\beta_3,\gamma,\lambda| \quad \text{relations} >$$

The relations are,

$$\begin{aligned}\alpha &= a_3d_2a_2^{-1}\\ \beta_1 &= a_2d_2^{-1}a_2a_3^{-1}a_2^{-1}\\ \beta_2 &= a_2a_1d_1^{-1}\\ \beta_3 &= a_1a_3d_3^{-1}\\ \gamma &= d_1a_2^{-1}a_1^{-1}\\ \lambda &= d_3a_1^{-1}a_3^{-1}\end{aligned}$$

Therefore,

$$\pi_1(A,x_0) =< a_1,a_2,a_3,d_1,d_2,d_3 >$$

The subspace B for the complement space for this structure gives us a ball with 6 axes removed, so there are six different untangled arcs in this subspace. Therefore, we need Six generators for these rods where the subspace B is a free group generated with these c_is.

$$\pi_1(B,x_0) \quad = \quad < c_1,c_2,c_3,c_4,c_5,c_6 >$$

In the same manner, the process of finding relations on $A\cap B$ will be repeated here for this cylinder packing ${}^{+}\Sigma$.

$$\begin{aligned}\pi_1(A\cap B,x_0) \quad &= \quad < L_{r_1},L_{r_2},L_{r_3},\overline{L_{r_1}},\overline{L_{r_2}},\overline{L_{r_3}},L_y,\overline{L_y},L_g,\overline{L_g},L_b,\overline{L_b},\\ &\quad | \quad \overline{L}_bL_gL_{r_3}L_yL_bL_{r_2}\overline{L}_gL_{r_1}\overline{L}_y\overline{L}_{r_1}\overline{L}_{r_2}\overline{L}_{r_3} >\end{aligned}$$

Therefore, one can represent the group of the complementary space of this cylinder packing as below group, which totally has 18 generators (see Tables 3.7, and 3.8);

$$\begin{aligned}\pi_1(\mathbb{T}^3\setminus{}^{+}\Sigma) \quad &= \quad < a_1,a_2,a_3,d_1,d_2,d_3,c_1,c_2,c_3,c_4,c_5,c_6| \quad a_3d_2a_2^{-1}c_4\\ &\quad , \quad a_1a_2d_2^{-1}a_3^{-1}a_1^{-1}c_3^{-1}c_5c_4^{-1}c_5^{-1}c_3, d_3a_1^{-1}a_3^{-1}c_6, a_2a_3a_1d_3^{-1}a_2^{-1}c_4c_6^{-1}c_4^{-1}\\ &\quad , \quad a_3a_2a_3^{-1}d_2^{-1}a_3^{-1}c_4^{-1}c_1c_4, a_3d_1a_1^{-1}a_2^{-1}a_3^{-1}c_4^{-1}c_1^{-1}c_4, a_2a_1d_1^{-1}c_2\\ &\quad , \quad a_2d_3a_3^{-1}a_1^{-1}a_2^{-1}c_2^{-1}, a_1a_3d_3^{-1}c_3, a_1a_2a_3a_2^{-1}d_2a_2^{-1}a_1^{-1}c_3^{-1}, d_1a_2^{-1}a_1^{-1}c_5\\ &\quad , \quad a_3a_1a_2d_1^{-1}a_3^{-1}c_6c_5^{-1}c_6^{-1} > . \qquad (3.4)\end{aligned}$$

Injective homomorphism I	Injective homomorphism J
$I(L_b) =< a_3 d_2 a_2^{-1} >$	$J(L_b) =< c_4^{-1} >$
$I(\overline{L_b}) =< a_1 a_2 d_2^{-1} a_3^{-1} a_1^{-1} >$	$J(\overline{L_b}) =< c_3^{-1} c_5 c_4^{-1} c_5^{-1} c_3 >$
$I(L_y) =< d_3 a_1^{-1} a_3^{-1} >$	$J(L_y) =< c_6^{-1} >$
$I(\overline{L_y}) =< a_2 a_3 a_1 d_3^{-1} a_2^{-1} >$	$J(\overline{L_y}) =< c_4 c_6 c_4^{-1} >$
$I(L_{r_1}) =< a_3 a_2 a_3^{-1} d_2^{-1} a_3^{-1} >$	$J(L_{r_1}) =< c_4^{-1} c_1^{-1} c_4 >$
$I(\overline{L_{r_1}}) =< a_3 d_1 a_1^{-1} a_2^{-1} a_3^{-1} >$	$J(\overline{L_{r_1}}) =< c_4^{-1} c_1 c_4 >$
$I(L_{r_2}) =< a_2 a_1 d_1^{-1} >$	$J(L_{r_2}) =< c_2^{-1} >$
$I(\overline{L_{r_2}}) =< a_2 d_3 a_3^{-1} a_1^{-1} a_2^{-1} >$	$J(\overline{L_{r_2}}) =< c_2 >$
$I(L_{r_3}) =< a_1 a_3 d_3^{-1} >$	$J(L_{r_3}) =< c_3^{-1} >$
$I(\overline{L_{r_3}}) =< a_1 a_2 a_3 a_2^{-1} d_2 a_2^{-1} a_1^{-1} >$	$J(\overline{L_{r_3}}) =< c_3 >$
$I(L_g) =< d_1 a_2^{-1} a_1^{-1} >$	$J(L_g) =< c_5^{-1} >$
$I(\overline{L_g}) =< a_3 a_1 a_2 d_1^{-1} a_3^{-1} >$	$J(\overline{L_g}) =< c_6 c_5 c_6^{-1} >$

Table 3.7: Injective homomorphism on the intersection of two subspaces in Theorem 3

$I(L_b)J(L_b)^{-1} =< a_3 d_2 a_2^{-1} c_4 >$	$I(\overline{L_b})J(\overline{L_b})^{-1} =< a_1 a_2 d_2^{-1} a_3^{-1} a_1^{-1} c_3^{-1} c_5 c_4^{-1} c_5^{-1} c_3 >$
$I(L_y)J(L_y)^{-1} =< d_3 a_1^{-1} a_3^{-1} c_6 >$	$I(\overline{L_y})J(\overline{L_y})^{-1} =< a_2 a_3 a_1 d_3^{-1} a_2^{-1} c_4 c_6^{-1} c_4^{-1} >$
$I(L_{r_1})J(L_{r_1})^{-1} =< a_3 a_2 a_3^{-1} d_2^{-1} a_3^{-1} c_4^{-1} c_1 c_4 >$	$I(\overline{L_{r_1}})J(\overline{L_{r_1}})^{-1} =< a_3 d_1 a_1^{-1} a_2^{-1} a_3^{-1} c_4^{-1} c_1^{-1} c_4 >$
$I(L_{r_2})J(L_{r_2})^{-1} =< a_2 a_1 d_1^{-1} c_2 >$	$I(\overline{L_{r_2}})J(\overline{L_{r_2}})^{-1} =< a_2 d_3 a_3^{-1} a_1^{-1} a_2^{-1} c_2^{-1} >$
$I(L_{r_3})J(L_{r_3})^{-1} =< a_1 a_3 d_3^{-1} c_3 >$	$I(\overline{L_{r_3}})J(\overline{L_{r_3}})^{-1} =< a_1 a_2 a_3 a_2^{-1} d_2 a_2^{-1} a_1^{-1} c_3^{-1} >$
$I(L_g)J(L_g)^{-1} =< d_1 a_2^{-1} a_1^{-1} c_5 >$	$I(\overline{L_g})J(\overline{L_g})^{-1} =< a_3 a_1 a_2 d_1^{-1} a_3^{-1} c_6 c_5^{-1} c_6^{-1} >$

Table 3.8: Relations on intersection of subspaces $A\&B$ for $^{+}\Sigma$

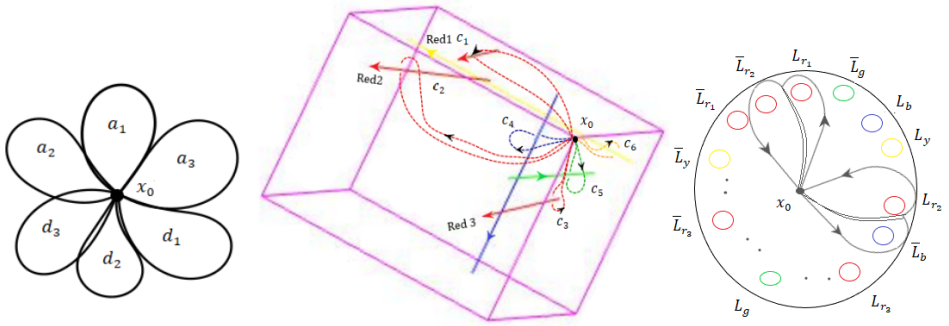

Figure 3.12: From left, subspace A, diagram of B with 13 generators, and homeomorphic image for $A \cap B$ which is the shell of a ball in the primitive cell includes cylinder axes removed for cylinder packing $^{+}\Sigma$

3.6 Computations for the group of the complementary space of ${}^{+}\Omega$

Next cylinder packing is ${}^{+}\Omega$, which has direction [111], symmetry $I432$, and axes:

$$\{(\frac{1}{3}+t,\frac{2}{3}+t,t);(\frac{2}{3}-t,\frac{1}{3}-t,t);(\frac{2}{3}+t,\frac{2}{3}-t,t);(\frac{1}{3}-t,\frac{1}{3}+t,t)\}$$

Similar to the previous cylinder packing, the orginal crystallography unit cell for this structure is a body-centered cubic cell that is non-primitive. By considering the same three basis vectors for all the other invarinat cylinder packings, we will have the pink primitive orhombohedral unit cell as in Figure (3.13). In this case, the internal axes will be Blue, green, yellow, and three reds:

$$\begin{aligned}\{\quad & (\frac{1}{3}+t,\frac{2}{3}+t,t);(\frac{1}{3}-t,\frac{4}{3}-t,t);(\frac{1}{3}-t,\frac{1}{3}+t,t)\\ ;\quad & (\frac{2}{3}+t,\frac{2}{3}-t,t+1);(\frac{2}{3}+t,\frac{2}{3}-t,t);(t-\frac{1}{3},\frac{2}{3}-t,t)\}\end{aligned}$$

Now by the equation of faces one can get the intersection points for axes with all

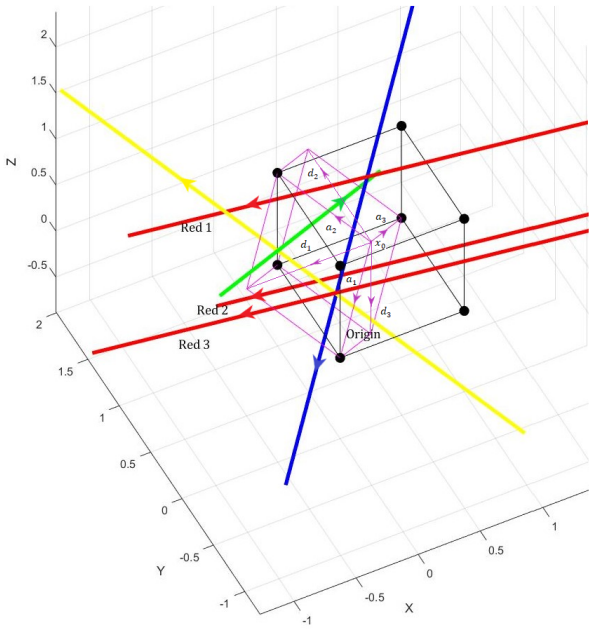

Figure 3.13: Cylinder packing ${}^{+}\Omega$ in rhombohedral primitive cell

Top, Bottom, Side 1 (left side), Side 2 (right side), Front, and Back faces;

- Blue rod goes from Top face to Bottom face:
  - Intersection point with Top face: $(\frac{2}{3},1,\frac{1}{3})$
  - Intersection point with Bottom face: $(\frac{1}{6},\frac{1}{2},-\frac{1}{6})$

- Green rod goes from Front face to the Back face:
  - Intersection point with the Front face: $(0, \frac{2}{3}, \frac{2}{3})$
  - Intersection point with the Back face: $(\frac{1}{2}, \frac{7}{6}, \frac{1}{6})$
- Yellow rod goes from the Side 2 face to the first side:
  - Intersection point with the second side is: $(\frac{1}{3}, \frac{1}{3}, 0)$
  - Intersection point with the first side is : $(-\frac{1}{6}, \frac{5}{6}, \frac{1}{2})$
- Red 1 goes from Top face to Side 1 face:
  - Intersection point with the Top face: $(\frac{1}{3}, 1, \frac{2}{3})$
  - Intersection point with the first side is: $(\frac{1}{6}, \frac{7}{6}, \frac{1}{2})$
- Red 2 goes from Side 2 to the Back face:
  - Intersection point with the second side face is : $(\frac{2}{3}, \frac{2}{3}, 0)$
  - Intersection point with Back face: $(\frac{1}{2}, \frac{5}{6}, -\frac{1}{6})$
- Red 3 goes from the Front face to the Bottom face:
  - Intersection point with Front face: $(0, \frac{1}{3}, \frac{1}{3})$
  - Intersection point with Bottom face; $(-\frac{1}{6}, \frac{1}{2}, \frac{1}{6})$

Therefore, the subspace A for the complementary space of ${}^{+}\Omega$ in the pink cell has two punctures in each face similar to ${}^{+}\Pi$ and ${}^{+}\Sigma$. The deformation retraction of this subspace is displayed in Figure (3.14) as the wedge of six circles which can be presented by six generators $\{a_1, a_2, a_3, d_1, d_2, d_3\}$. Again, we can represent these circles by the original generators a_i, d_j as the following relations

$$\pi_1(A, x_0) =< a_1, a_2, a_3, d_1, d_2, d_3, \alpha, \beta_1, \beta_2, \beta_3, \gamma, \lambda | \quad \text{relations} >$$

The relations are as the following,

$$\alpha = a_3 a_2 d_2^{-1}$$

$$\beta_1 = d_2 a_3^{-1} a_2^{-1}$$

$$\beta_2 = d_3 a_1^{-1} a_3^{-1}$$

$$\beta_3 = d_1 a_2^{-1} a_1^{-1}$$

$$\gamma = a_2 a_1 d_1^{-1}$$

$$\lambda = a_1 a_3 d_3^{-1}$$

Therefore,

$$\pi_1(A, x_0) =< a_1, a_2, a_3, d_1, d_2, d_3 >$$

The second subspace B will be a ball with all the axes, which will be the diagram in Figure (3.14). In this diagram, all information about how the axes go under or over each other are also achieved by looking at the cell from direction [111], so we get a projection of this onto a plane along direction [111] which means the diagonal plane of its primitive unit cell. See Figure (3.15) which shows the relations for these five crossings. We found the relations by Wirtinger presentation as explained in Section 2.3.1.

$$\begin{aligned}\pi_1(B,x_0) &= < c_1,c_2,c_3,c_4,...,c_{11} | c_{10}^{-1}c_7c_5c_7^{-1}, c_6^{-1}c_5^{-1}c_8c_5, c_8^{-1}c_4c_9c_4^{-1} \\ &, \quad c_5^{-1}c_4c_1c_4^{-1}, c_4c_2c_3^{-1}c_2^{-1} >\end{aligned}$$

Now same process will be repeated to find out the relations on the intersection between two subspaces A and B for cylinder packings ${}^{+}\Omega$.

$$\begin{aligned}\pi_1(A\cap B,x_0) &= < L_{r_1}, L_{r_2}, L_{r_3}, \overline{L_{r_1}}, \overline{L_{r_2}}, \overline{L_{r_3}}, L_y, L_g\overline{L_g}, L_b, \overline{L_b}, \\ &| \quad \overline{L}_bL_{r_2}L_yL_b\overline{L}_gL_{r_1}\overline{L}_{r_2}\overline{L}_{r_1}\overline{L}_y\overline{L}_{r_3}L_gL_{r_3} >\end{aligned}$$

Injective homomorphism I	Injective homomorphism J
$I(L_b) =< a_3a_2d_2^{-1} >$	$J(L_b) =< c_{10}^{-1} >$
$I(\overline{L_b}) =< a_1d_2a_2^{-1}a_3^{-1}a_1^{-1} >$	$J(\overline{L_b}) =< c_1 >$
$I(L_y) =< a_1a_3d_3^{-1} >$	$J(L_y) =< c_2^{-1}c_3^{-1}c_2 >$
$I(\overline{L_y}) =< a_2d_3a_3^{-1}a_1^{-1}a_2^{-1} >$	$J(\overline{L_y}) =< c_4 >$
$I(L_{r_1}) =< d_2a_3^{-1}a_2^{-1} >$	$J(L_{r_1}) =< c_{11}^{-1} >$
$I(\overline{L_{r_1}}) =< a_2a_3a_1d_3^{-1}a_2^{-1} >$	$J(\overline{L_{r_1}}) =< c_{11} >$
$I(L_{r_2}) =< d_3a_1^{-1}a_3^{-1} >$	$J(L_{r_2}) =< c_6^{-1} >$
$I(\overline{L_{r_2}}) =< a_3a_1a_2d_1^{-1}a_3^{-1} >$	$J(\overline{L_{r_2}}) =< c_7c_{10}^{-1}c_4c_9c_4^{-1}c_{10}c_7^{-1} >$
$I(L_{r_3}) =< d_1a_2^{-1}a_1^{-1} >$	$J(L_{r_3}) =< c_2^{-1} >$
$I(\overline{L_{r_3}}) =< a_1a_2a_3d_2^{-1}a_1^{-1} >$	$J(\overline{L_{r_3}}) =< c_2 >$
$I(L_g) =< a_2a_1d_1^{-1} >$	$J(L_g) =< c_7^{-1} >$
$I(\overline{L_g}) =< a_3d_1a_1^{-1}a_2^{-1}a_3^{-1} >$	$J(\overline{L_g}) =< c_{10}^{-1}c_7c_{10} >$

Table 3.9: Injective homomorphism on the intersection of two subspaces in Theorem 3

From Tables 3.9, and 3.10, the final representation for the fundamental group of

$I(L_b)J(L_b)^{-1} =< a_3a_2d_2^{-1}c_{10} >$	$I(\overline{L_b})J(\overline{L_b})^{-1} =< a_1d_2a_2^{-1}a_3^{-1}a_1^{-1}c_1 >$
$I(L_y)J(L_y)^{-1} =< a_1a_3d_3^{-1}c_2^{-1}c_3c_2 >$	$I(\overline{L_y})J(\overline{L_y})^{-1} =< a_2d_3a_3^{-1}a_1^{-1}a_2^{-1}c_4^{-1} >$
$I(L_{r_1})J(L_{r_1})^{-1} =< d_2a_3^{-1}a_2^{-1}c_{11} >$	$I(\overline{L_{r_1}})J(\overline{L_{r_1}})^{-1} =< a_2a_3a_1d_3^{-1}a_2^{-1}c_{11}^{-1} >$
$I(L_{r_2})J(L_{r_2})^{-1} =< d_3a_1^{-1}a_3^{-1}c_6 >$	$I(\overline{L_{r_2}})J(\overline{L_{r_2}})^{-1} =< a_3a_1a_2d_1^{-1}a_3^{-1}c_7c_{10}^{-1}c_4c_9^{-1}c_4^{-1}c_{10}c_7^{-1} >$
$I(L_{r_3})J(L_{r_3})^{-1} =< d_1a_2^{-1}a_1^{-1}c_2 >$	$I(\overline{L_{r_3}})J(\overline{L_{r_3}})^{-1} =< a_1a_2a_3d_2^{-1}a_1^{-1}c_2^{-1} >$
$I(L_g)J(L_g)^{-1} =< a_2a_1d_1^{-1}c_7 >$	$I(\overline{L_g})J(\overline{L_g})^{-1} =< a_3d_1a_1^{-1}a_2^{-1}a_3^{-1}c_{10}^{-1}c_7^{-1}c_{10} >$

Table 3.10: Relations on intersection of subspaces $A\&B$ for ${}^+\Omega$

the complementary space for ${}^+\Omega$ is as below

$$\begin{aligned}\pi_1(\mathbb{T}^3 \setminus {}^+\Omega) \quad = \quad & < a_1, a_2, a_3, d_1, d_2, d_3, c_1, c_2, c_3, c_4, ..., c_{11} | \quad c_{10}^{-1}c_7c_5c_7^{-1}, c_6^{-1}c_5^{-1}c_8c_5 \\ & , \quad c_8^{-1}c_4c_9c_4^{-1}, c_5^{-1}c_4c_1c_4^{-1}, c_4c_2c_3^{-1}c_2^{-1}, a_3a_2d_2^{-1}c_{10}, a_1d_2a_2^{-1}a_3^{-1}a_1^{-1}c_1^{-1} \\ & , \quad a_1a_3d_3^{-1}c_2^{-1}c_3c_2, a_2d_3a_3^{-1}a_1^{-1}a_2^{-1}c_4^{-1}, d_2a_3^{-1}a_2^{-1}c_{11} \\ & , \quad a_2a_3a_1d_3^{-1}a_2^{-1}c_{11}^{-1}, d_3a_1^{-1}a_3^{-1}c_6, a_3a_1a_2d_1^{-1}a_3^{-1}c_7c_{10}^{-1}c_4c_9^{-1}c_4^{-1}c_{10}c_7^{-1} \\ & , \quad d_1a_2^{-1}a_1^{-1}c_2, a_1a_2a_3d_2^{-1}a_1^{-1}c_2^{-1}, a_2a_1d_1^{-1}c_7 \\ & , \quad a_3d_1a_1^{-1}a_2^{-1}a_3^{-1}c_{10}^{-1}c_7^{-1}c_{10} > . \end{aligned} \tag{3.5}$$

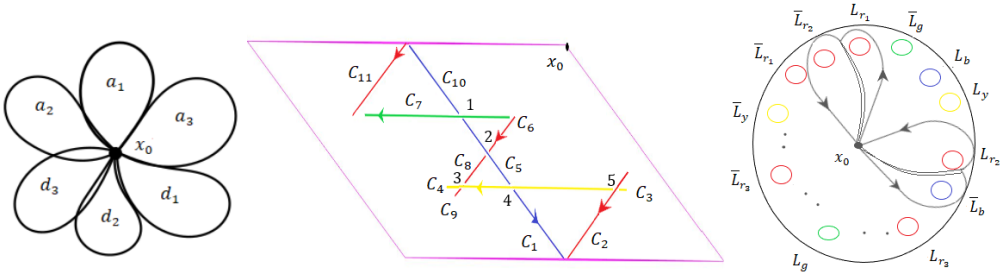

Figure 3.14: From left, subspace A, diagram of B with 11 generators, and homeomorphic image for $A \cap B$ which is the shell of a ball in the primitive cell includes cylinder axes removed for cylinder packing ${}^+\Omega$

3.7 Computations for the group of the complementary space of $\Sigma^\star$

The final invariant cylinder packing with symmetry $Ia\bar{3}d$ is $\Sigma^\star$, which is the intergrowth of ${}^+\Sigma$ and its enantiomorph ${}^-\Sigma$ with symmetry $I4_132$ and axes;

$$\{(\frac{2}{3}+t, \frac{1}{3}+t, t); (\frac{1}{3}-t, \frac{1}{6}-t, t); (\frac{5}{6}+t, \frac{1}{3}-t, t); (\frac{1}{6}-t, \frac{1}{6}+t, t)\}$$

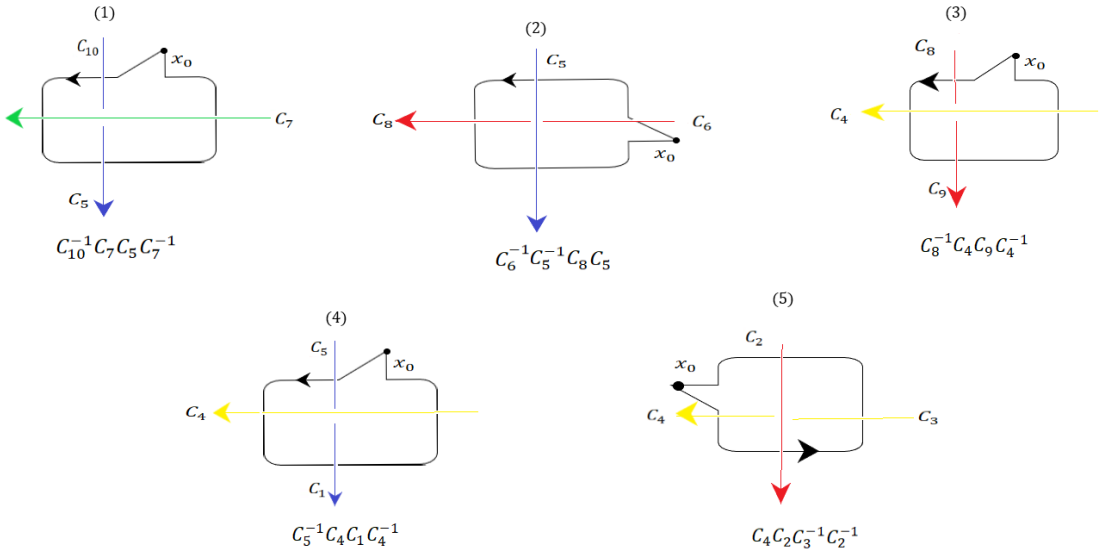

Figure 3.15: Five crossings in the diagram of the subspace B for the complementary space of cylinder packing ${}^{+}\Omega$ which is shown in Figure (3.14)

These axes are the result of some symmetry operations such as reflections and translations of the axes for ${}^{+}\Sigma$.

The symmetry of $\Sigma^{\star}$ is $Ia\bar{3}d$ with again direction $[111]$, so we need to construct the primitive orhombohedral cell as well as other cylinder packings. As you can see in Figure(3.16), the internal axes in this unit cell are first Reds, Greens, Blues, and Yellows as following;

$$\begin{aligned}
\{\quad & (\tfrac{1}{6}+t,\tfrac{7}{6}-t,t);(\tfrac{1}{6}+t,\tfrac{2}{3}-t,t+1);(\tfrac{1}{6}+t,\tfrac{2}{3}-t,t)\\
;\quad & (\tfrac{5}{6}+t,\tfrac{1}{3}-t,t+1);(\tfrac{5}{6}+t,\tfrac{1}{3}-t,t);(\tfrac{5}{6}+t,-\tfrac{2}{3}-t,t+1)\\
;\quad & (\tfrac{1}{3}-t,\tfrac{7}{6}-t,t);(\tfrac{2}{3}-t,\tfrac{5}{6}-t,t);(-\tfrac{1}{3}+t,\tfrac{1}{3}+t,t)\\
;\quad & (\tfrac{1}{3}+t,\tfrac{2}{3}+t,t);(\tfrac{5}{6}-t,\tfrac{5}{6}+t,t);(\tfrac{1}{6}-t,\tfrac{1}{6}+t,t)\}
\end{aligned}$$

Again by the equations of the primitive cell faces, one can reach the intersection points with the internal axes.

- Red 1 goes from the Top face to the Back face, and intersection points are $(\frac{7}{12},\frac{5}{4},\frac{5}{12})$, $(\frac{1}{2},\frac{4}{3},\frac{1}{3})$.
- Red 2 goes from the Front face to the first (left) Side, and intersection points are $(0,\frac{5}{6},\frac{5}{6})$, $(-\frac{1}{12},\frac{11}{12},\frac{3}{4})$.
- Red 3 goes from the second (right) Side to the Bottom face, and intersection

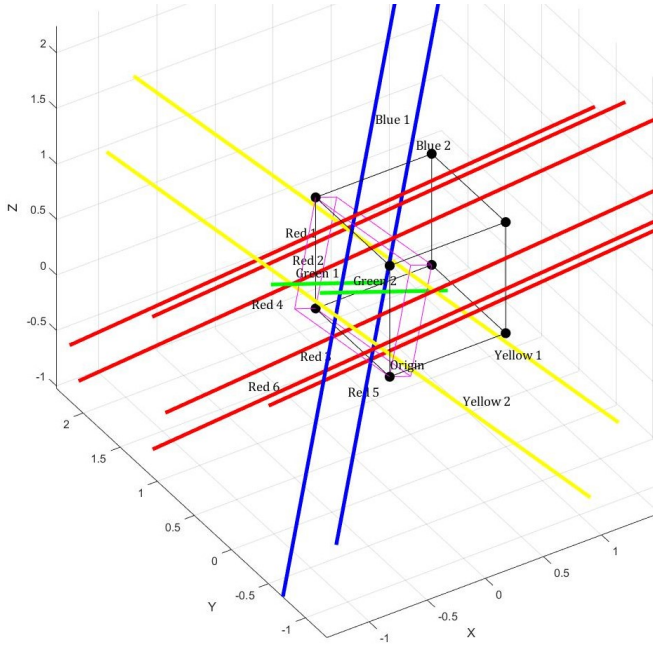

Figure 3.16: Cylinder packing $\Sigma^\star$ in rhombohedral primitive cell

points are $(\frac{5}{12}, \frac{5}{12}, \frac{1}{4})$, $(\frac{1}{12}, \frac{3}{4}, -\frac{1}{12})$.

- Red 4 goes from the Top face to the first Side face, and intersection points are $(\frac{5}{12}, \frac{3}{4}, \frac{7}{12})$, $(\frac{1}{12}, \frac{13}{12}, \frac{1}{4})$.
- Red 5 goes from the second Side to the Back face, and intersection points are $(\frac{7}{12}, \frac{7}{12}, -\frac{1}{4})$, $(\frac{1}{2}, \frac{2}{3}, -\frac{1}{3})$.
- Red 6 goes from the Front face to the Bottom face, and intersection points are $(0, \frac{1}{6}, \frac{1}{6})$, $(-\frac{1}{12}, \frac{1}{4}, \frac{1}{12})$.
- Green 1 goes from the Front face to the Back face, and intersection points are $(-\frac{1}{4}, \frac{7}{12}, \frac{7}{12})$, $(\frac{1}{4}, \frac{13}{12}, \frac{1}{12})$.
- Green 2 goes from the Front face to the Back face, and intersection points are $(\frac{1}{4}, \frac{5}{12}, \frac{5}{12})$, $(\frac{3}{4}, \frac{11}{12}, -\frac{1}{12})$.
- Blue 1 goes from the Top face to the Bottom face, and intersection points are $(\frac{1}{3}, 1, \frac{2}{3})$, $(-\frac{1}{6}, \frac{1}{2}, \frac{1}{6})$.
- Blue 2 goes from the Top face to the Bottom face, and intersection points are $(\frac{2}{3}, 1, \frac{1}{3})$, $(\frac{1}{6}, \frac{1}{2}, -\frac{1}{6})$.
- Yellow 1 goes from the second Side to the first Side, and the intersection points are $(\frac{5}{6}, \frac{5}{6}, 0)$, $(\frac{1}{3}, \frac{4}{3}, \frac{1}{2})$.
- Yellow 2 again goes from the Side 2 to the Side 1 face, and intersection points are, $(\frac{1}{6}, \frac{1}{6}, 0)$, $(-\frac{1}{3}, \frac{2}{3}, \frac{1}{2})$.

It is clear that in this case the number of punctures in each face of the primitive cell is actually four. Similarly, one can present the deformation retraction of this subspace to the wedge of 12 circles, with 12 generators. In this case, we can combine the loops on each face by a relation with the original generators of the three-torus $\{a_1, a_2, a_3\}$.

$$\begin{aligned}\pi_1(A, x_0) &= < \alpha_1, \alpha_2, \beta_1, \ldots, \beta_6, \lambda_1, \lambda_2, \gamma_1, \gamma_2, a_1, a_2, a_3 | \quad \alpha_2\beta_1\beta_4\alpha_1 a_2 a_3 a_2^{-1} a_3^{-1} \\ &, \quad \beta_2\gamma_1\gamma_2\beta_6 a_1 a_2 a_1^{-1} a_2^{-1}, \lambda_2\beta_3\beta_5\lambda_1 a_3 a_1 a_3^{-1} a_1^{-1} >\end{aligned}$$

For subspace B here we consider 6 crossings with 18 generators, which we determined by the projection of this primitive cell onto a diagonal plane which its normal unit vector field is in direction $[101]$. The diagram is shown in Figure (3.17), and the crossings with their relations by Wirtinger presentation in Figure (3.18).

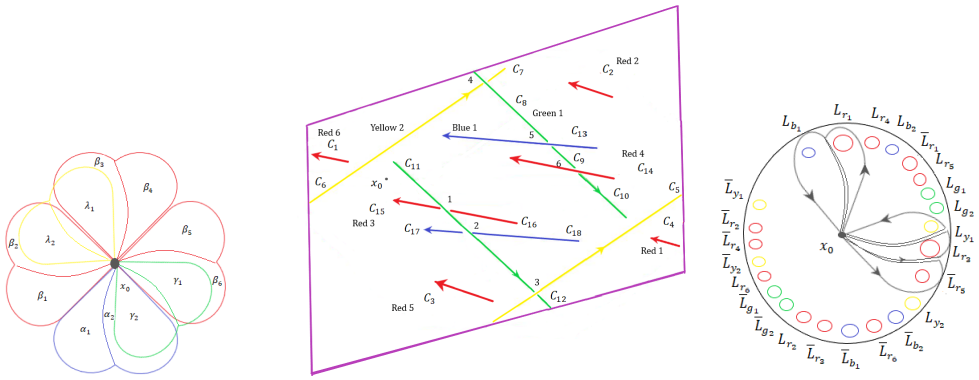

Figure 3.17: From left subspace A, the diagram of subspace B, and $A \cap B$ for cylinder packing $\Sigma^\star$

$$\begin{aligned}\pi_1(B, x_0) &= < c_1, \ldots, c_{18} | \quad c_{15}c_{11}c_{16}^{-1}c_{11}^{-1}, c_{17}c_{11}c_{18}^{-1}c_{11}^{-1} \\ &, \quad c_5^{-1}c_{12}c_5c_{11}^{-1}, c_8c_7c_8^{-1}c_6^{-1}, c_9c_{13}^{-1}c_8^{-1}c_{13}, c_{10}c_{14}^{-1}c_9^{-1}c_{14} >\end{aligned}$$

And now the process to find the relations on the intersection of two subspaces will be repeated. However, because here we have more than two punctures in each face of the pink unit cell, the loops L_i on the intersection parts related to the subspace A can not be expressed by a_i and d_j as before.

$$\begin{aligned}\pi_1(A \cap B, x_0) &= < L_{r_1}, L_{r_2}, L_{r_3}, L_{r_4}, L_{r_5}, L_{r_6}, \overline{L}_{r_1}, \overline{L}_{r_2}, \overline{L}_{r_3}, \overline{L}_{r_4}, \overline{L}_{r_5}, \overline{L}_{r_6} \\ &, \quad L_{y_1}, L_{y_2}, \overline{L}_{y_1}, \overline{L}_{y_2}, L_{g_1}, L_{g_2}, \overline{L}_{g_1}, \overline{L}_{g_2}, L_{b_1}, L_{b_2}, \overline{L}_{b_1}, \overline{L}_{b_2}, \\ &| \quad \overline{L}_{b_1}\overline{L}_{r_6}\overline{L}_{b_2}L_{y_2}\overline{L}_{r_5}L_{r_3}L_{y_1}L_{g_2}L_{g_1}L_{r_5}\overline{L}_{r_1}L_{b_2}L_{r_4}L_{r_1}L_{b_1}\overline{L}_{y_1} \\ &. \quad \overline{L}_{r_2}\overline{L}_{r_4}\overline{L}_{y_2}L_{r_6}\overline{L}_{g_1}\overline{L}_{g_2}L_{r_2}\overline{L}_{r_3} >\end{aligned}$$

So the final representation for the fundamental group of complementary space of

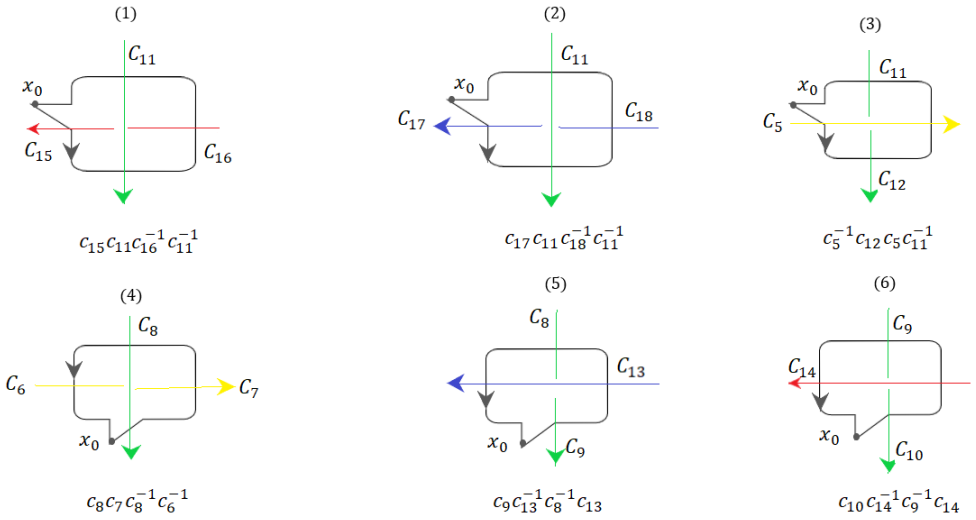

Figure 3.18: 6 crossings and their relations on subspace B for complementary space of $\Sigma^\star$

$I(L_{b_1})J(L_{b_1})^{-1} =< \alpha_1 c_{13} >$	$I(\overline{L_{b_1}})J(\overline{L_{b_1}})^{-1} =< a_1\alpha_1^{-1}a_1^{-1}c_1c_6^{-1}c_{11}c_{13}^{-1}c_{11}^{-1}c_6c_1^{-1} >$
$I(L_{b_2})J(L_{b_2})^{-1} =< \alpha_2 c_{18} >$	$I(\overline{L_{b_2}})J(\overline{L_{b_2}})^{-1} =< a_1\alpha_2^{-1}a_1^{-1}c_6^{-1}c_{16}^{-1}c_{11}c_{17}^{-1}c_{11}^{-1}c_{16}c_6 >$
$I(L_{r_1})J(L_{r_1})^{-1} =< \beta_1 c_4 >$	$I(\overline{L_{r_1}})J(\overline{L_{r_1}})^{-1} =< a_3\beta_2^{-1}a_3^{-1}c_{18}^{-1}c_4^{-1}c_{18} >$
$I(L_{r_2})J(L_{r_2})^{-1} =< \beta_2 c_2 >$	$I(\overline{L_{r_2}})J(\overline{L_{r_2}})^{-1} =< a_2\beta_3^{-1}a_2^{-1}c_2^{-1} >$
$I(L_{r_3})J(L_{r_3})^{-1} =< \beta_3 c_{16} >$	$I(\overline{L_{r_3}})J(\overline{L_{r_3}})^{-1} =< a_1\beta_1^{-1}a_1^{-1}c_7^{-1}c_{15}^{-1}c_7 >$
$I(L_{r_4})J(L_{r_4})^{-1} =< \beta_4 c_{14} >$	$I(\overline{L_{r_4}})J(\overline{L_{r_4}})^{-1} =< a_2\beta_5^{-1}a_2^{-1}c_{13}c_{14}^{-1}c_{13}^{-1} >$
$I(L_{r_5})J(L_{r_5})^{-1} =< \beta_5 c_3 >$	$I(\overline{L_{r_5}})J(\overline{L_{r_5}})^{-1} =< a_2\beta_6^{-1}a_2^{-1}c_5c_3^{-1}c_5^{-1} >$
$I(L_{r_6})J(L_{r_6})^{-1} =< \beta_6 c_1 >$	$I(\overline{L_{r_6}})J(\overline{L_{r_6}})^{-1} =< a_1\beta_4^{-1}a_1^{-1}c_1^{-1} >$
$I(L_{g_1})J(L_{g_1})^{-1} =< \gamma_1 c_8 >$	$I(\overline{L_{g_1}})J(\overline{L_{g_1}})^{-1} =< a_3\gamma_1^{-1}a_3^{-1}c_5c_{18}^{-1}c_{13}^{-1}c_{10}^{-1}c_{13}c_{18}c_5^{-1} >$
$I(L_{g_2})J(L_{g_2})^{-1} =< \gamma_2 c_{11} >$	$I(\overline{L_{g_2}})J(\overline{L_{g_2}})^{-1} =< a_3\gamma_2^{-1}a_3^{-1}c_5c_{12}^{-1}c_5^{-1} >$
$I(L_{y_1})J(L_{y_1})^{-1} =< \lambda_1 c_5 >$	$I(\overline{L_{y_1}})J(\overline{L_{y_1}})^{-1} =< a_2\lambda_1^{-1}a_2^{-1}c_{13}c_{14}c_{18}c_5^{-1}c_{18}^{-1}c_{14}^{-1}c_{13}^{-1} >$
$I(L_{y_2})J(L_{y_2})^{-1} =< \lambda_2 c_6 >$	$I(\overline{L_{y_2}})J(\overline{L_{y_2}})^{-1} =< a_2\lambda_2^{-1}a_2^{-1}c_2^{-1}c_8^{-1}c_{11}^{-1}c_7^{-1}c_{11}c_8c_2 >$

Table 3.11: Relations on intersection of subspaces $A\&B$ for $\Sigma^\star$

cylinder packing $\Sigma^\star$ with respect to the primitive rhombohedral cell in Figure (3.16) and relations from the Table 3.11 is as the following representation;

$$\begin{aligned}
\pi_1(\mathbb{T}^3 \setminus \Sigma^\star) &= < a_1, a_2, a_3, c_1, , ..., c_{18}, \alpha_1, \alpha_2, \beta_1, \ldots, \beta_6, \gamma_1, \gamma_2, \lambda_1, \lambda_2 | c_{15} c_{11} c_{16}^{-1} c_{11}^{-1} \\
&, \; c_9 c_{13}^{-1} c_8^{-1} c_{13}, c_8 c_7 c_8^{-1} c_6^{-1}, c_{17} c_{11} c_{18}^{-1} c_{11}^{-1}, c_{10} c_{14}^{-1} c_9^{-1} c_{14}, c_5^{-1} c_{12} c_5 c_{11}^{-1} \\
&, \; \alpha_1 c_{13}, a_1 \alpha_1^{-1} a_1^{-1} c_1 c_6^{-1} c_{11} c_{13}^{-1} c_{11}^{-1} c_6 c_1^{-1}, \alpha_2 c_{18}, a_1 \alpha_2^{-1} a_1^{-1} c_6^{-1} c_{16}^{-1} c_{11} c_{17}^{-1} c_{11}^{-1} c_{16} c_6 \\
&, \; \beta_1 c_4, a_3 \beta_2^{-1} a_3^{-1} c_{18}^{-1} c_4^{-1} c_{18}, \beta_2 c_2, a_2 \beta_3^{-1} a_2^{-1} c_2^{-1}, \beta_3 c_{16}, a_1 \beta_1^{-1} a_1^{-1} c_7^{-1} c_{15}^{-1} c_7 \\
&, \; \beta_4 c_{14}, a_2 \beta_5^{-1} a_2^{-1} c_{13} c_{14}^{-1} c_{13}, \beta_5 c_3, a_2 \beta_6^{-1} a_2^{-1} c_5 c_3^{-1} c_5^{-1}, \beta_6 c_1, a_1 \beta_4^{-1} a_1^{-1} c_1^{-1} \\
&, \; \gamma_1 c_8, a_3 \gamma_1^{-1} a_3^{-1} c_5 c_{18}^{-1} c_{13}^{-1} c_{10}^{-1} c_{13} c_{18} c_5^{-1}, \gamma_2 c_{11}, a_3 \gamma_2^{-1} a_3^{-1} c_5 c_{12}^{-1} c_5^{-1}, \lambda_1 c_5 \\
&, \; a_2 \lambda_1^{-1} a_2^{-1} c_{13} c_{14} c_{18} c_5^{-1} c_{18}^{-1} c_{14}^{-1} c_{13}^{-1}, \lambda_2 c_6, a_2 \lambda_2^{-1} a_2^{-1} c_2^{-1} c_8^{-1} c_{11}^{-1} c_7^{-1} c_{11} c_8 c_2 \\
&, \; \alpha_2 \beta_1 \beta_4 \alpha_1 a_2 a_3 a_2^{-1} a_3^{-1}, \beta_2 \gamma_1 \gamma_2 \beta_6 a_1 a_2 a_1^{-1} a_2^{-1}, \lambda_2 \beta_3 \beta_5 \lambda_1 a_3 a_1 a_3^{-1} a_1^{-1} > . \quad (3.6)
\end{aligned}$$

The group presentations in equations (1), (2), (3), (4), (5), and (6) are the group of six invariant cylinder packings. In the following Section, we determine if these groups are algebraically isomorphic or non-isomorphic.

3.8 The invariants of the finitely presented groups

The computations in the last section resulted in six finitely presented groups. Now we need to show these groups are non-isomorphic groups. In this regard, this will prove that the complementary space of these links in $\mathbb{T}^3$ are inequivalent, which guarantees that these crystalline materials are distinct links in the three-torus. But the problem of determining when two of these fundamental groups are isomorphic or non-isomorphic is generally difficult [Hatcher, 2001]. Here, we use the program "GAP", [Group, 2019], and the function LowIndexSubgroupsFpGroup which is used to find all subgroups of a finitely presented group up to a given index. This function can be used to make analysis of the finitely presented groups more computationally feasible, as the subgroups provide information about the structure of the group. Additionally, there are finitely many subgroups of up to a given index in any finitely presented group. This was done for knot complements by [Brendel et al., 2015].

We compute subgroups of the fundamental group with at least index 2 and 3 using GAP, where all have different number of subgroups with index at most 3, and this is shown that all these finitely presented groups (fundamental groups) are distinct.

This distinction proves that all these six structures are inequivalence links in the three-torus because their complements can not be homeomorphic, see Table 3.12.

Symbol	Index 2	Index 3
Π^*	8	36
${}^+\Pi$	16	43
Γ	16	80
${}^+\Sigma$	16	87
${}^+\Omega$	16	81
Σ^*	256	7786

Table 3.12: All numbers of Subgroups for fundamental groups of complement of cylinder packings with at least index 2 and 3

Figures (3.19), (3.20), (3.21), (3.22), (3.23), and (3.24) show the related codes for computing the number of subgroups at most index 2 and 3 in GAP.

```
gap> F:=FreeGroup(6);
<free group on the generators [ f1, f2, f3, f4, f5, f6 ]>
gap> G:=F/[F.3*F.2*F.3^-1*F.2^-1*F.5,F.3*F.1*F.3^-1*F.2*F.3*F.2^-1*F.1^-1*F.3^-1*F.5^-
1,F.2*F.1*F.2^-1*F.1^-1*F.6^-1*F.4*F.6,F.3*F.1*F.2*F.1^-1*F.2^-1*F.3^-1*F.5^-1*F.4^-
1*F.5,F.1*F.3*F.1^-1*F.3^-1*F.6,F.2*F.3*F.1*F.3^-1*F.1^-1*F.2^-1*F.6^-1];
<fp group on the generators [ f1, f2, f3, f4, f5, f6 ]>
gap> L:=LowIndexSubgroupsFpGroup(G,2);;
gap> Length(L);
8
gap> P:=LowIndexSubgroupsFpGroup(G,3);;
gap> Length(P);
36
```

Figure 3.19: Low index subgroups of $\Pi^{\star}$

```
gap> F:=FreeGroup(12);
<free group on the generators [ f1, f2, f3, f4, f5, f6, f7, f8, f9, f10, f11, f12 ]>
gap> G:=F/[F.5*F.3^-1*F.2^-1*F.11^-1*F.7*F.11,F.3*F.1*F.2*F.4^-1*F.3^-1*F.7^-1,F.2*F.1*F.4^-
1*F.12,F.4*F.3*F.5^-1*F.2*F.4^-1*F.12^-1,F.2*F.6*F.3^-1*F.1^-1*F.2^-1*F.11,F.3*F.2*F.5^-1*F.11^-
1,F.1*F.5*F.2^-1*F.3^-1*F.1^-1*F.8,F.1*F.3*F.6^-1*F.8^-1,F.6*F.1^-1*F.3^-1*F.9,F.3*F.4*F.1^-
1*F.2^-1*F.3^-1*F.9^-1,F.4*F.2^-1*F.1^-1*F.10,F.2*F.3*F.1*F.6^-1*F.2^-1*F.10^-1];
<fp group on the generators [ f1, f2, f3, f4, f5, f6, f7, f8, f9, f10, f11, f12 ]>
gap> L:=LowIndexSubgroupsFpGroup(G,2);;
gap> Length(L);
16
gap> P:=LowIndexSubgroupsFpGroup(G,3);;
gap> Length(P);
43
```

Figure 3.20: Low index subgroups of ${}^{+}\Pi$

```
gap> F:=FreeGroup(12);
<free group on the generators [ f1, f2, f3, f4, f5, f6, f7, f8, f9, f10, f11, f12 ]>
gap> G:=F/[F.3*F.2*F.5^-1*F.8,F.1*F.5*F.2^-1*F.3^-1*F.1^-1*F.8^-1,F.1*F.3*F.6^-1*F.9,F.2*F.6*F.3^-
1*F.1^-1*F.2^-1*F.11^-1*F.8*F.9^-1*F.8^-1*F.11,F.4*F.2^-1*F.1^-1*F.7,F.1*F.2*F.3*F.5^-1*F.1^-
1*F.7^-1,F.6*F.1^-1*F.3^-1*F.10,F.3*F.1*F.2*F.4^-1*F.3^-1*F.10^-1,F.5*F.3^-1*F.2^-
1*F.12,F.2*F.3*F.1*F.6^-1*F.2^-1*F.12^-1,F.2*F.1*F.4^-1*F.11,F.3*F.4*F.1^-1*F.2^-1*F.3^-
1*F.8^-1*F.11^-1*F.8];
<fp group on the generators [ f1, f2, f3, f4, f5, f6, f7, f8, f9, f10, f11, f12 ]>
gap> L:=LowIndexSubgroupsFpGroup(G,2);;
gap> Length(L);
16
gap> P:=LowIndexSubgroupsFpGroup(G,3);;
gap> Length(P);
80
```

Figure 3.21: Low index subgroups of Γ

```
gap> F:=FreeGroup(17);
<free group on the generators [ f1, f2, f3, f4, f5, f6, f7, f8, f9, f10, f11, f12, f13, f14, f15,
f16, f17 ]>
gap> G:=F/[F.16^-1*F.13*F.11*F.13^-1,F.12^-1*F.11^-1*F.14*F.11,F.14^-1*F.10*F.15*F.10^-1,F.11^-
1*F.10*F.7*F.10^-1,F.10*F.8*F.9^-1*F.8^-1,F.3*F.2*F.5^-1*F.16,F.1*F.5*F.2^-1*F.3^-1*F.1^-1*F.7^-
1,F.1*F.3*F.6^-1*F.8^-1*F.9*F.8,F.2*F.6*F.3^-1*F.1^-1*F.2^-1*F.10^-1,F.5*F.3^-1*F.2^-
1*F.17,F.2*F.3*F.1*F.6^-1*F.2^-1*F.17^-1,F.6*F.1^-1*F.3^-1*F.12,F.3*F.1*F.2*F.4^-1*F.3^-
1*F.13*F.16^-1*F.10*F.15^-1*F.10^-1*F.16*F.13^-1,F.4*F.2^-1*F.1^-1*F.8,F.1*F.2*F.3*F.5^-1*F.1^-
1*F.8^-1,F.2*F.1*F.4^-1*F.13,F.3*F.4*F.1^-1*F.2^-1*F.3^-1*F.16^-1*F.13^-1*F.16];
<fp group on the generators [ f1, f2, f3, f4, f5, f6, f7, f8, f9, f10, f11, f12, f13, f14, f15,
f16, f17 ]>
gap> L:=LowIndexSubgroupsFpGroup(G,2);;
gap> Length(L);
16
gap> P:=LowIndexSubgroupsFpGroup(G,3);;
gap> Length(P);
81
```

Figure 3.22: Low index subgroups of ${}^{+}\Omega$

```
gap> F:=FreeGroup(12);
<free group on the generators [ f1, f2, f3, f4, f5, f6, f7, f8, f9, f10, f11, f12 ]>
gap> G:=F/[F.3*F.5*F.2^-1*F.10,F.1*F.2*F.5^-1*F.3^-1*F.1^-1*F.9^-1*F.11*F.10^-
1*F.11^-1*F.9,F.6*F.1^-1*F.3^-1*F.12,F.2*F.3*F.1*F.6^-1*F.2^-1*F.10*F.12^-1*F.10^-
1,F.3*F.2*F.3^-1*F.5^-1*F.3^-1*F.10^-1*F.7*F.10,F.3*F.4*F.1^-1*F.2^-1*F.3^-1*F.10^-
1*F.7^-1*F.10,F.2*F.1*F.4^-1*F.8,F.2*F.6*F.3^-1*F.1^-1*F.2^-1*F.8^-1,F.1*F.3*F.6^-
1*F.9,F.1*F.2*F.3*F.2^-1*F.5*F.2^-1*F.1^-1*F.9^-1,F.4*F.2^-1*F.1^-
1*F.11,F.3*F.1*F.2*F.4^-1*F.3^-1*F.12*F.11^-1*F.12^-1];
<fp group on the generators [ f1, f2, f3, f4, f5, f6, f7, f8, f9, f10, f11, f12 ]>
gap> L:=LowIndexSubgroupsFpGroup(G,2);;
gap> Length(L);
16
gap> P:=LowIndexSubgroupsFpGroup(G,3);;
gap> Length(P);
87
```

Figure 3.23: Low index subgroups of ${}^{+}\Sigma$

```
gap> F:=FreeGroup(33);
<free group with 33 generators>
gap> G:=F/[F.18*F.14*F.19^-1*F.14^-1,F.20*F.14*F.21^-1*F.14^-1,F.8^-1*F.15*F.8*F.14^-
1,F.11*F.10*F.11^-1*F.9^-1,F.12*F.16^-1*F.11^-1*F.16,F.13*F.17^-1*F.12^-
1*F.17,F.22*F.16,F.1*F.22^-1*F.1^-1*F.4*F.9^-1*F.14*F.16^-1*F.14^-1*F.9*F.4^-
1,F.23*F.21,F.1*F.23^-1*F.1^-1*F.9^-1*F.19^-1*F.14*F.20^-1*F.14^-
1*F.19*F.9,F.24*F.7,F.3*F.25^-1*F.3^-1*F.21^-1*F.7^-1*F.21,F.25*F.5,F.2*F.26^-1*F.2^-
1*F.5^-1,F.26*F.19,F.1*F.24^-1*F.1^-1*F.10^-1*F.18^-1*F.10,F.27*F.17,F.2*F.28^-1*F.2^-
1*F.16*F.17^-1*F.16^-1,F.28*F.6,F.3*F.29^-1*F.3^-1*F.8*F.6^-1*F.8^-1,F.29*F.4,F.1*F.27^-
1*F.1^-1*F.4^-1,F.30*F.11,F.3*F.30^-1*F.3^-1*F.8*F.21^-1*F.16^-1*F.13^-1*F.16*F.21*F.8^-
1,F.31*F.14,F.3*F.31^-1*F.3^-1*F.8*F.15^-1*F.8^-1,F.32*F.8,F.2*F.32^-1*F.2^-
1*F.16*F.17*F.21*F.8^-1*F.21^-1*F.17^-1*F.16^-1,F.33*F.9,F.2*F.33^-1*F.2^-1*F.5^-1*F.11^-
1*F.14^-1*F.10^-1*F.14*F.11*F.5,F.23*F.24*F.27*F.22*F.2*F.3*F.2^-1*F.3^-
1,F.25*F.30*F.31*F.29*F.1*F.2*F.1^-1*F.2^-1,F.33*F.26*F.28*F.32*F.3*F.1*F.3^-1*F.1^-1];
<fp group with 33 generators>
gap> L:=LowIndexSubgroupsFpGroup(G,2);;
gap> Length(L);
256
gap> P:=LowIndexSubgroupsFpGroup(G,3);;
gap> Length(P);
7786
```

Figure 3.24: Low index subgroups of $\Sigma^{\star}$

3.9 Comparing Two structures From [Rosi et al., 2005]

Now we want to compute the same invariant for two structures, one layered and one parallel structure in Table 2.1 which Rosi et al. [2005] presented and then Evans et al. [2013] found an isotopy between them by applying the PB-SONO algorithm.

For structure number #1 in Rosi et al. [2005], there are two parallel axes in the unit cell where we calculate this fundamental group, so in each subspace we have the following relations and generators

$$\pi_1(A, x_0) =< a_1, a_2, a_3, d \mid \quad a_2 a_1 a_2^{-1} a_1^{-1}, a_1 a_3 a_1^{-1} a_3^{-1} >$$
$$\pi_1(B, x_0) =< c_1, c_2 >$$

The intersection between these two subspaces is again 4 different loops for each puncture which we have after removing axes in the complement, the relations are in Table 3.13 and 3.14.

$$\begin{aligned} \pi_1(A \cap B, x_0) \quad &= \quad < L_{b_1}, \overline{L_{b_1}}, L_{b_2}, \overline{L_{b_2}} \\ &\quad \mid \quad L_{b_1} L_{b_2} \overline{L_{b_2} L_{b_1}} > \end{aligned}$$

Injective homomorphism I	Injective homomorphism J
$I(L_{b_1}) =< a_3 a_2 d^{-1} >$	$J(L_{b_1}) =< c_1^{-1} >$
$I(\overline{L_{b_1}}) =< a_1 d a_2^{-1} a_3^{-1} a_1^{-1} >$	$J(\overline{L_{b_1}}) =< c_1 >$
$I(L_{b_2}) =< d a_3^{-1} a_2^{-1} >$	$J(L_{b_2}) =< c_2^{-1} >$
$I(\overline{L_{b_1}}) =< a_1 a_2 a_3 d^{-1} a_1^{-1} >$	$J(\overline{L_{b_1}}) =< c_2 >$

Table 3.13: Injective homomorphisms on the intersection of two subspaces as mentioned in Theorem 3

$I(L_{b_1}) J(L_{b_1})^{-1} =< a_3 a_2 d^{-1} c_1 >$	$I(\overline{L_{b_1}}) J(\overline{L_{b_1}})^{-1} =< a_1 d a_2^{-1} a_3^{-1} a_1^{-1} c_1^{-1} >$
$I(L_{b_2}) J(L_{b_2})^{-1} =< d a_3^{-1} a_2^{-1} c_2 >$	$I(\overline{L_{b_2}}) J(\overline{L_{b_2}})^{-1} =< a_1 a_2 a_3 d^{-1} a_1^{-1} c_2^{-1} >$

Table 3.14: Relations on intersection of subspaces $A\&B$ for structure number #1 in Rosi et al. [2005]

$$\begin{aligned} \pi_1(\mathbb{T}^3 \setminus \text{Structure \#1}) \quad &= \quad < a_1, a_2, a_3, d, c_1, c_2 | a_3 a_2 d^{-1} c_1^{-1}, a_1 d a_2^{-1} a_3^{-1} a_1^{-1} c_1^{-1} \\ &\quad , \quad d a_3^{-1} a_2^{-1} c_2, a_1 a_2 a_3 d^{-1} a_1^{-1} c_2^{-1}, a_1 a_3 a_1^{-1} a_3^{-1} \\ &\quad , \quad a_2 a_1 a_2^{-1} a_1^{-1} > . \end{aligned}$$

See Figure (3.25), to see the generators.

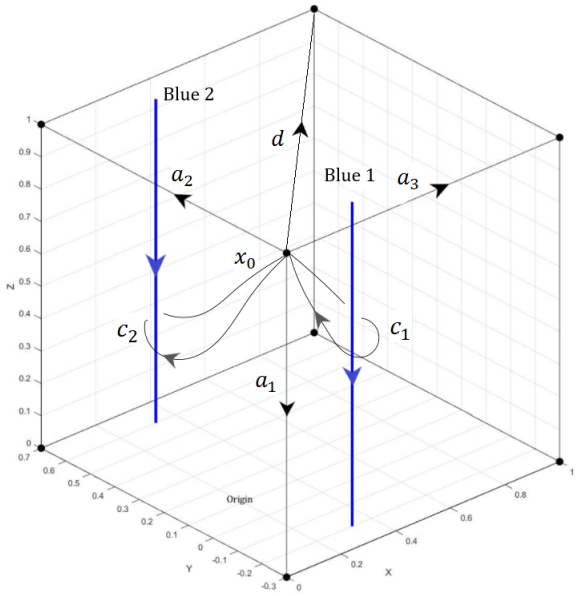

Figure 3.25: Structure number #1 which is a parallel cylinder packing in Rosi et al. [2005]

The number of subgroups for this group with at least index 2 is 16 (see Figure (3.26).

```
gap> F:=FreeGroup(6);
<free group on the generators [ f1, f2, f3, f4, f5, f6 ]>
gap> G:=F/[F.3*F.2*F.6^-1*F.4^-1,F.1*F.6*F.2^-1*F.3^-1*F.1^-1*F.4^-1,F.6*F.3^-
1*F.2^-1*F.5,F.1*F.2*F.3*F.6^-1*F.1^-1*F.5^-1,F.1*F.3*F.1^-1*F.3^-1,F.2*F.1*F.2^-1*F.1^-1];
<fp group on the generators [ f1, f2, f3, f4, f5, f6 ]>
gap> P:=LowIndexSubgroupsFpGroup(G,2);;
gap> Length(P);
16
```

Figure 3.26: Low index subgroups of structure number #1 in Rosi et al. [2005]

Now for structure number #6 in Rosi et al. [2005], there are layered axes in the unit cell where we calculate this fundamental group, so in each subspace we have the following relations and generators

The fundamental group of the first subspace A which is the wedge of two circles, (see Figure (3.4)), that can be written as the following relations:

$$\pi_1(A, x_0) =< a_1, a_2, a_3, \alpha, \beta | \quad \alpha = a_3 a_2 a_3^{-1} a_2^{-1}, \beta = a_1 a_3 a_1^{-1} a_3^{-1}, a_2 a_1 a_2^{-1} a_1^{-1} >$$

So the group can be rewritten;

$$\pi_1(A, x_0) =< a_1, a_2, a_3 | \quad a_2 a_1 a_2^{-1} a_1^{-1} >$$

The second subspace deformation retracts to a ball with two different untangled arcs, so the fundamental group of this subspace is achieved by two different loops or

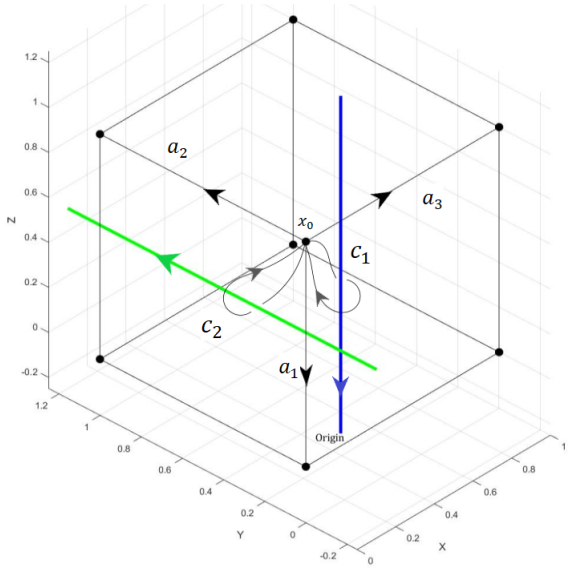

Figure 3.27: Structure number #6 which is a layered cylinder packing in Rosi et al. [2005]

generators from basepoint x_0 which can track each rod independently, in this point we can say $\pi_1(B)$ is just a free group generated by two loops c_1, and c_2.

$$\pi_1(B, x_0) =< c_1, c_2 >$$

Now the relations with respect to the intersection of these two subspaces is a spherical shell with loops L_{t_i} and $\overline{L_{t_i}}$ as the generators, where t represents the first letter of the colour of the axis. With respect to the direction, when the axis enters the cell we selected the first symbol L_{t_i}, and when it exits we used the second symbol $\overline{L_{t_i}}$. In this notation the relations on the intersection of two subspaces A and B are;

$$\begin{aligned} \pi_1(A \cap B, x_0) \quad &= \quad < L_g, \overline{L_g}, L_b, \overline{L_b} \\ &\quad | \quad \overline{L}_b L_g L_b \overline{L}_g > \end{aligned}$$

Injective homomorphism I	Injective homomorphism J
$I(L_b) =< a_3 a_2 a_3^{-1} a_2^{-1} >$	$J(L_b) =< c_1^{-1} >$
$I(\overline{L_b}) =< a_3 a_1 a_3^{-1} a_2 a_3 a_2^{-1} a_1^{-1} a_3^{-1} >$	$J(\overline{L_b}) =< c_1 >$
$I(L_g) =< a_1 a_3 a_1^{-1} a_3^{-1} >$	$J(L_g) =< c_2^{-1} >$
$I(\overline{L_g}) =< a_2 a_3 a_1 a_3^{-1} a_1^{-1} a_2^{-1} >$	$J(\overline{L_g}) =< c_2 >$

Table 3.15: Injective homomorphisms on the intersection of two subspaces as mentioned in Theorem 3

$I(L_b)J(L_b)^{-1} =< a_3a_2a_3^{-1}a_2^{-1}c_1 >$	$I(\overline{L_b})J(\overline{L_b})^{-1} =< a_3a_1a_3^{-1}a_2a_3a_2^{-1}a_1^{-1}a_3^{-1}c_1^{-1} >$
$I(L_g)J(L_g)^{-1} =< a_1a_3a_1^{-1}a_3^{-1}c_2 >$	$I(\overline{L_g})J(\overline{L_g})^{-1} =< a_2a_3a_1a_3^{-1}a_1^{-1}a_2^{-1}c_2^{-1} >$

Table 3.16: Relations on intersection of subspaces $A\&B$ for structure number #6 in Rosi et al. [2005]

Therefore, the final presentation of the complementary space for this cylinder packing will be as following, where we can see the relations are derived in Table 3.15 and 3.16

$$\begin{aligned}\pi_1(\mathbb{T}^3 \setminus \text{Structure \#6}) \quad &= \quad < a_1, a_2, a_3, c_1, c_2 | \quad a_3a_2a_3^{-1}a_2^{-1}c_1, a_3a_1a_3^{-1}a_2a_3a_2^{-1}a_1^{-1}a_3^{-1}c_1^{-1} \\ &, \quad a_1a_3a_1^{-1}a_3^{-1}c_2, a_2a_3a_1a_3^{-1}a_1^{-1}a_2^{-1}c_2^{-1}, a_2a_1a_2^{-1}a_1^{-1} > .\end{aligned}$$

The number of subgroups with at least index 2 calculated in Figure (3.28), which is 8.

```
gap> F:=FreeGroup(5);
<free group on the generators [ f1, f2, f3, f4, f5 ]>
gap> G:=F/[F.3*F.2*F.3^-1*F.2^-1*F.4,F.3*F.1*F.3^-1*F.2*F.3*F.2^-1*F.1^-1*F.3^-1*F.4^-
1,F.1*F.3*F.1^-1*F.3^-1*F.5,F.2*F.3*F.1*F.3^-1*F.1^-1*F.2^-1*F.5^-1,F.2*F.1*F.2^-1*F.1^-1];
<fp group on the generators [ f1, f2, f3, f4, f5 ]>
gap> P:=LowIndexSubgroupsFpGroup(G,2);;
gap> Length(P);
8
```

Figure 3.28: Low index subgroups of structure number #6 in Rosi et al. [2005]

Therefore, these two structures are different from each other because the number of subgroups for the fundamental groups of their complement are different. As a result, these two structures are not equivalent mathematically although Evans et al. [2013] showed physical equivalency between them by the simulation.

Chapter 4

Link complement problem

In the previous chapter, we used the fact that if the complement of links in a 3-manifold are distinct, links must be inequivalent. Now this important question arises "Does the complementary space define the link?" or in other words if the complementary space of two links in a 3-manifold are homeomorphic, are the links equivalent.

There are many studies about the knot and link complements, but in 1989 Gordon and Luecke answered this question for knots and links of course with some restrictions [Whitehead, 1937]&[Gordon, 2002]. We look at some of the related theorems here.

Theorem 4 *.[Gordon and Luecke, 1989] Two prime knots in $\mathbb{S}^3$ are equivalent if and only if the complementary spaces have isomorphic fundamental groups.*

The proof of Theorem 4 used results about constructing 3-manifolds via Dehn surgery on knots in $\mathbb{S}^3$ which we do not explain here.

Theorem 4 is false for links in $\mathbb{S}^3$ [Whitehead, 1937]&[Rolfsen, 1976]. Two distinct links can have homeomorphic complementary spaces. Take two links as shown in Figure 4.1, the first created by linking two copies of the unknot (J and K), and the second created by linking an unknot, J, with trefoil, K'.

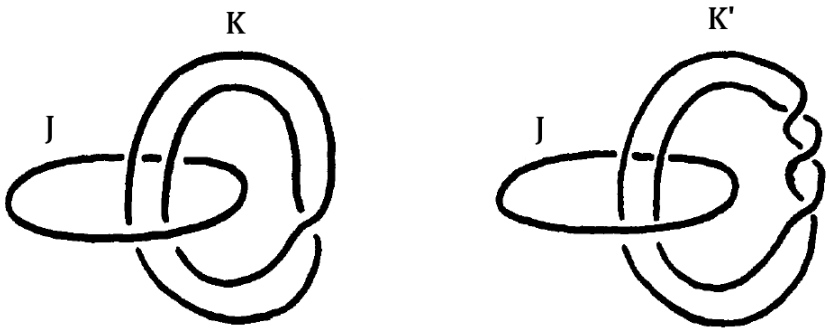

Figure 4.1: Two inequivalent links with homeomorphic complements [Rolfsen, 1976], L_1 on the left and L_2 on the right

Both links have linking number 2, with orientation from left to right. Thus they are nontrivial. But they cannot be equivalent, because the trefoil is nontrivial. Here

we suppose $L_1 \neq L_2$, and show $\mathbb{S}^3 \setminus L_1 \cong \mathbb{S}^3 \setminus L_2$. The unknot's complement in the three-sphere is a solid torus, so we can view both K and K' as curves in the solid torus in Figure (4.2). By applying twist homeomorphism

$$h : \mathbb{S}^1 \times \mathbb{B}^2 \subset \mathbb{C}^2 \to \mathbb{S}^1 \times \mathbb{B}^2 \subset \mathbb{C}^2$$

$$h(z, w) = (z, zw)$$

where (z, w) is in $\mathbb{C}^2$, carries K into K' by a homeomorphism of $\mathbb{S}^3 \setminus J$. It follows that $\mathbb{S}^3 \setminus L_1 = (J \cup K)$ and $\mathbb{S}^3 \setminus L_2 = (J \cup K')$ are homeomorphic.

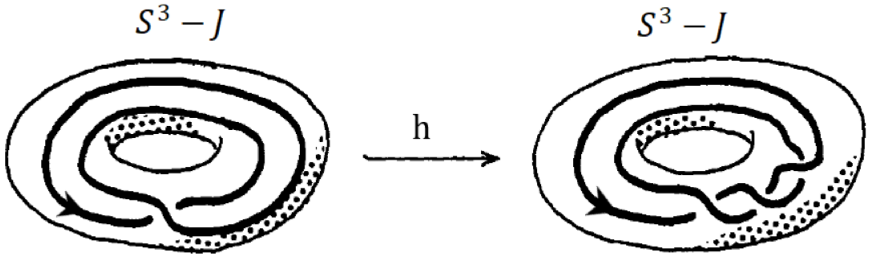

Figure 4.2: Two knot complements in a solid torus [Rolfsen, 1976]

We want to generalise this technique for our case in the three-torus, first we need to consider a similar twist homeomorphism in a subset of $\mathbb{T}^3$. In the above example Rolfsen [1976] used the Heegaard splitting of $\mathbb{S}^3$ and handlebodies in this splitting which are two solid tori. Now before using the same method in $\mathbb{T}^3$, we describe Heegaard splitting for general 3-manifolds and how we can split the three-torus.

Mathematicians sometimes represent closed, orientable three-manifolds by splitting them into two handlebodies of genus g and an orientation preserving homemorphism of their boundary surfaces; the manifold can be constructed as the result of gluing via that homeomorphism. This splitting is called Heegaard splitting for 3-manifolds.

Definition 6 *.Johnson [2006]. A Heegaard splitting for a 3-manifold M is an ordered triple (Σ, H_1, H_2) where Σ is a closed surface embedded in M and H_1 and H_2 are handlebodies embedded in M such that $\partial H_1 = \Sigma = \partial H_2 = H_1 \cap H_2$ and $H_1 \cup H_2 = M$. The surface Σ is called a Heegaard surface. The Heegaard genus of M is the smallest possible genus of a Heegaard splitting of M.*

Manifolds usually do not have a unique splitting, and can be represented with splitting of different genus, but in each case both handlebodies have the same genus. For example for $\mathbb{S}^3$, for any non-negative integer g there is a Heegaard splitting of this genus g [Scharlemann, 2000]. Usually, the Heegaard splitting of $\mathbb{S}^3$ with genus 1 is used for different aspects like Dehn surgery and knot theory. The complement of a solid torus V_1 in $\mathbb{S}^3$ is another solid torus V_2 which contains a point at infinity, and we can write $\mathbb{S}^3 = V_1 \cup V_2$, where Σ from Definition 6 is a homeomorphism which maps the longitude curve of V_1 to the meridian curve of V_2. This gives us the idea of

splitting $\mathbb{S}^3$ in two handlebodies with genus 1, which are two solid torus; see Figure (4.3).

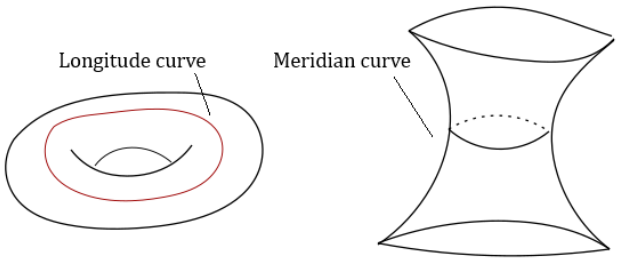

Figure 4.3: Genus 1 Heegaard splitting for the three-sphere, which is two solid tori glued along the red longitude curve of the solid torus V_1 on the left to the black meridian curve of the other one V_2 on the right side

Waldhausen (1968) showed that all splittings of the 3-sphere are standard, and that this was also shown for the 3-torus by Boileau et al. [1990].

Now, we explain the standard Heegaard splitting for the 3-torus with genus 3, then use this for constructing two different links in this manifold with the homeomorphic complement as Whitehead [1937] did for the links in $\mathbb{S}^3$.

Suppose C is a cube presenting the three-torus by identifying opposite faces of the cube $[0,1] \times [0,1] \times [0,1]$. So another representaion for the three-torus is $S^1 \times S^1 \times S^1$. Let $\phi : C \to \mathbb{T}^3$ be the map induced by the map $[0,1] \to S^1$, which takes eight vertices of the cube to a vertex $v \in \mathbb{T}^3$. Parallel edges in C map to the same edge in $\mathbb{T}^3$ so the 12 edges of the cube map to three edges in $\mathbb{T}^3$. Therefore consider a graph such as K which is built with these three edges and a vertex v in $\mathbb{T}^3$. Let N be a regular neighborhood of this graph and H_2 be the complement of N. The pre-image $\phi^{-1}(H_2)$ is topologically a ball in the cube, shown in Figure (4.4). The faces of the cube intersect H_2 in disks which chop H_2 into this ball $\phi^{-1}(H_2)$, so H_2 is a handlebody.

Because N is a regular neighborhood of a graph, its closure H_1 is also a handlebody. If σ is the surface $H_1 \cap H_2$ then (σ, H_1, H_2) is a Heegaard splitting for the three-torus with genus 3 [Scharlemann, 2000].

We generalise the counterexample of inequivalent links in $\mathbb{S}^3$ with homeomorphic complement to our case of the three-torus by the following steps.

First, consider a trivial loop in the three-torus which we break into four pieces inside the unit cell so that it intersects the top and bottom faces, right and left sides of the cube. This trivial component is completely inside the handlebody H_1. Now we want to have a twisting along the solid arm (or branch) of the part of H_1 that intersects the top face, so we have a tangled structure in Figure (4.5) part b. By considering this twist, which is a full clockwise rotation, the twisted H_1 is still homeomorphic to the original form of this handlebody. This homeomorphism is a twist homeomorphism of H_1.

Second, consider two links $L_1 = K_1 \cup U$ and $L_2 = K_2 \cup U$ in Figure (4.6), where U

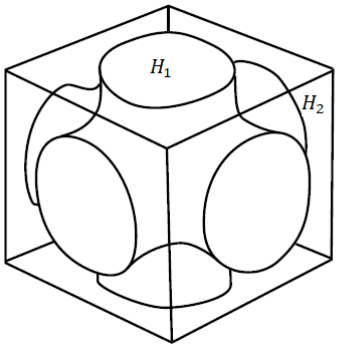

Figure 4.4: Standard Heegaard splitting for the three-torus with two handlebodies H_1 and H_2 [Scharlemann, 2000]

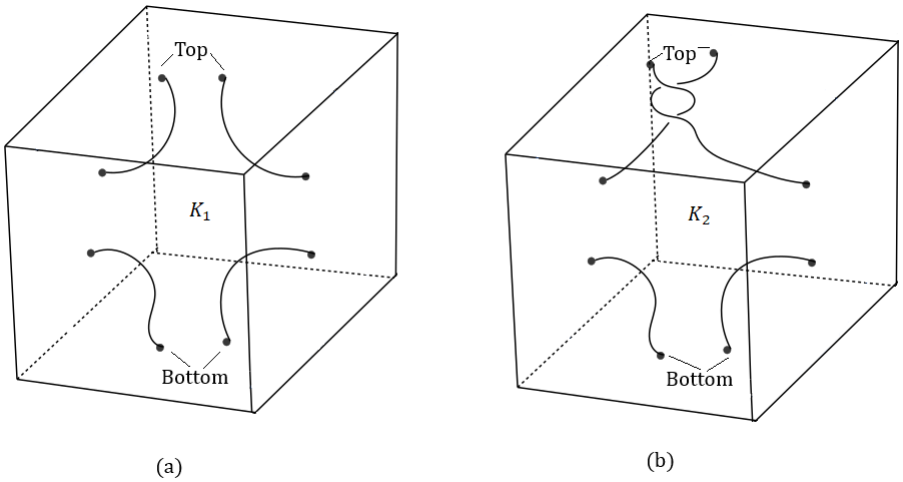

Figure 4.5: (a) Trivial knot in handlebody H_1, (b) The image of K_1 after one full twist of the top arm of H_1

is a simple unknot lying wholly within H_2, and U is a kind of dual to the twist which lies in the horizontal plane but the twist happens in a thickened slab. We consider the complement of these links in the 3-torus. By sitting U in the horizontal slab and removing a neighbourhood of U, we cut the slab into two pieces; a disk where the twist occurs, and the rest which is homotopic to a wedge of two circles. Now from above we have a twisting homeomorphism in H_1 and because the components K_1 and K_2 are both completely inside H_1, we can extend this homeomorphism into $\mathbb{T}^3 \setminus U$. This shows the complemetary space of U in the two examples are homeomorphic. And consequently the spaces $\mathbb{T}^3 \setminus L_1$ and $\mathbb{T}^3 \setminus L_2$ are homeomorphic.

Finally, we want to show these two links are not equivalent although their complements were homeomorphic.

One component (unknot) inside H_2 in both links are identical, so we compare these two links by just looking at the their second components. After projecting

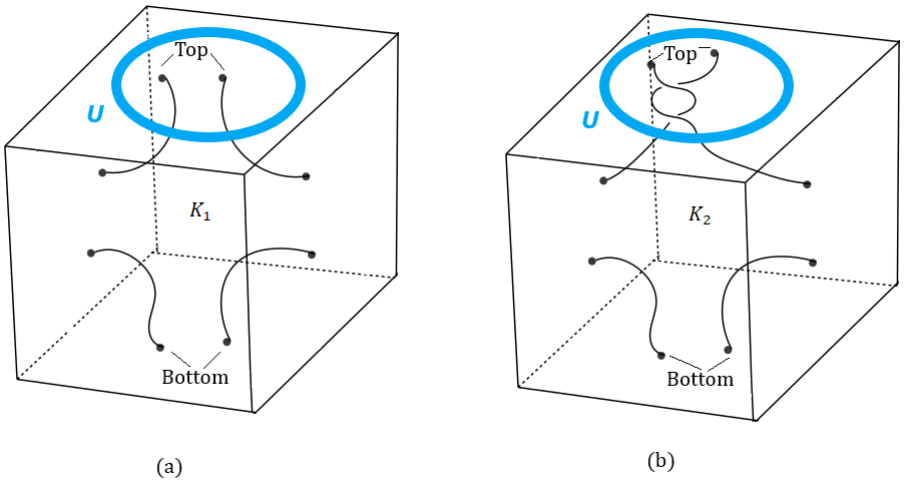

Figure 4.6: Two distinct links L_1 and L_2 in the 3-torus with homeomorphic complement by using twist homeomorphism on H_1

these structures along the coordinate axis perpendicular to the plane of K_1 and K_2, they can be taken as the 2-periodic structures in the thickened torus $\mathbb{T}^2 \times I$ which is homotopic to $\mathbb{T}^2$. According to this projection, one can get the following 2D-patterns. Clearly, both have one component per unit cell with the same crossing number zero, but one of these patterns is just a periodic trivial loop with linking number zero (Figure (4.7) on the left) and the other one is a nontrivial with linking number 2 (Figure (4.7) on the right), which is notated in Grishanov et al. [2009] by *lks* per unit cell.

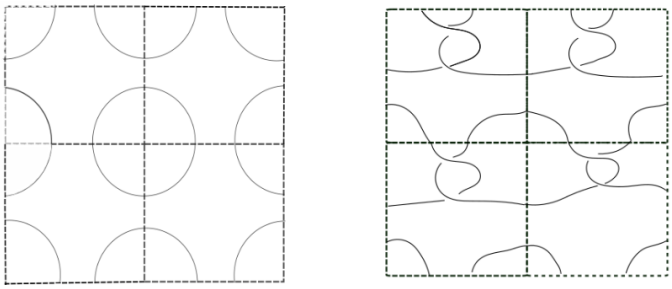

Figure 4.7: Projection of components K_1 and K_2 of links L_1 and L_2 onto the thickened torus

Therefore, we constructed two different links with homeomorphic complements in the 3-torus, so generalisation is completed. We can claim here that links in the three-torus cannot be determined by their complements, same as links in $\mathbb{S}^3$.

Chapter 5

Conclusion

In this thesis, we considered six invariant cubic rod packings [O'Keeffe et al., 2001] as six links in the three-torus, and by comparing the computed fundamental groups of their complements, proved that these structures are non-isotopic links in this manifold.

First, we found the primitive unit cell for ${}^{+}\Pi$, Γ, ${}^{+}\Sigma$, ${}^{+}\Omega$, and $\Sigma^{\star}$; then we used Van-Kampen Theorem and Wirtinger presentation method for the computations. Second, by comparing the number of subgroups of these computed finitely presented groups with the specific index by GAP, one can conclude all these algebraic groups are non-isomorphic. As a result, the complementary space of links in $\mathbf{T}^3$ is a nice resource to determine if these links are not equivalent. Therefore, we have the following Theorem,

Theorem 5 *The six cylinder packings with invariant position of axes in cubic symmetry in O'Keeffe et al. [2001], where the axes are along directions either* $[111] or [100]$*, are all inequivalent links in the three-torus (*$\mathbb{T}^3$*).*

Finally, we address this problem that links in the three-torus cannot be determined by their complements. That means if two links have the homeomorphic complements, they are not necessarily equivalent. In this regard, by presenting a contradiction included using twist homeomorphism in a handle-body with genus 3 from the three-torus, we proved that it is not possible to recognise that two links are necessarily equivalent if their complements are homeomorphic, which is the same result that was reported in Whitehead [1937] about links in the different 3-manifold $\mathbb{S}^3$.

5.1 Future Work

There are some works that can extend this study to more complicated cases of computing invariants for other crystalline materials;

- Computing the same invariant for more complex periodic structures with a single component which can be seen as knots in the three-torus or the structure in Figure (2.14), and see whether the Van-Kampen approach will be suitable for these structures.

- Finding an algorithm which is able to compute the fundamental groups of any periodic structures (not manually, because the technique that we used will be impossible for more complex structures.)
- Or computing other invariants might be useful to discriminate the more complicated structures that Evans et al. [2013] enumerated.

Bibliography

Boileau, M.; Otal, J.-P.; et al., 1990. Sur les scindements de heegaard du tore three-torus. *Journal of Differential Geometry*, 32, 1 (1990), 209–233. (cited on page 59)

Brendel, P.; Dłotko, P.; Ellis, G.; Juda, M.; and Mrozek, M., 2015. Computing fundamental groups from point clouds. *Applicable Algebra in Engineering, Communication and Computing*, 26, 1-2 (2015), 27–48. (cited on page 49)

Engel, P.; Michel, L.; and Senechal, M., 2004. Lattice geometry. Technical report. (cited on page 24)

Evans, M. E.; Robins, V.; and Hyde, S. T., 2013. Periodic entanglement ii: weavings from hyperbolic line patterns. *Acta Crystallographica Section A*, 69, 3 (2013), 262–275. (cited on pages ix, xiv, 19, 20, 52, 55, and 64)

Evans, M. E.; Robins, V.; and Hyde, S. T., 2015. Ideal geometry of periodic entanglements. *Proc. R. Soc. A*, 471, 2181 (2015), 20150254. (cited on pages xiii, 3, 12, and 19)

Fleming, P., 2016. Computing invariants of knotted graphs. (cited on page 1)

Friedrichs, O. D.; O Keeffe, M.; and Yaghi, O. M., 2003. Three-periodic nets and tilings: regular and quasiregular nets. *ACTA CRYSTALLOGRAPHICA SECTION A FOUNDATIONS OF CRYSTALLOGRAPHY*, 59, 1 (2003), 22–27. (cited on page 5)

Gordon, C., 2002. Links and their complements. *Contemporary Mathematics*, 314 (2002), 71–82. (cited on page 57)

Gordon, C. and Luecke, J., 1989. Knots are determined by their complements. *Journal of the American Mathematical Society*, 2, 2 (1989), 371–415. (cited on pages 9 and 57)

Grishanov, S.; Meshkov, V.; and Omelchenko, A., 2009. A topological study of textile structures. part i: An introduction to topological methods. *Textile Research Journal*, 79, 8 (2009), 702–713. (cited on pages ix, xiii, 5, 11, 16, 17, and 61)

Group, T. G., 2019. Gap - groups, algorithms, and programming, version 4.10.2. *(https://www.gap-system.org)*, (2019). (cited on page 49)

Hahn, T.; Shmueli, U.; and Arthur, J. W., 1983. *International tables for crystallography*, vol. 1. Reidel Dordrecht. (cited on page 17)

Hatcher, A., 2001. *Algebraic topology*. Cambridge University Press. (cited on pages xiii, 1, 6, 7, 11, 21, and 49)

Johnson, J., 2006. Notes on heegaard splittings. *Preprint*, (2006). (cited on pages ix and 58)

Johnson, J., 2011. Automorphisms of the three-torus preserving a genus-three heegaard splitting. *Pacific journal of mathematics*, 253, 1 (2011), 75–94. (cited on page 24)

Kauffman, L. H., 1993. Knots and physics, world scientific publishing co. *Pte. Ltd*, (1993). (cited on pages xiii, 5, and 8)

Kauffman, L. H. and Lambropoulou, S., 2012. Hard unknots and collapsing tangles. *Introductory lectures on knot theory, Ser. Knots Everything*, 46 (2012), 187–247. (cited on pages xiii, 7, and 8)

Lickorish, W. R., 2012. *An introduction to knot theory*, vol. 175. Springer Science & Business Media. (cited on page 7)

Ockwig, N. W.; Delgado-Friedrichs, O.; O'Keeffe, M.; and Yaghi, O. M., 2005. Reticular chemistry: occurrence and taxonomy of nets and grammar for the design of frameworks. *Accounts of chemical research*, 38, 3 (2005), 176–182. (cited on pages ix and 5)

O'Keeffe, M. and Andersson, S., 1977. Rod packings and crystal chemistry. *Acta Crystallographica Section A: Crystal Physics, Diffraction, Theoretical and General Crystallography*, 33, 6 (1977), 914–923. (cited on pages xvii, 1, 3, 14, and 15)

O'Keeffe, M.; Plévert, J.; Teshima, Y.; Watanabe, Y.; and Ogama, T., 2001. The invariant cubic rod (cylinder) packings: symmetries and coordinates. *Acta Crystallographica Section A: Foundations of Crystallography*, 57, 1 (2001), 110–111. (cited on pages ix, xiii, xvii, 1, 2, 3, 14, 18, 20, and 63)

Pierański, P., 1998. In search of ideal knots. *Computational Methods in Science and Technology*, 4 (1998), 9–23. (cited on pages xiv, 19, and 20)

Raymond, L. W., 1997. *Introduction to Knot Theory*. Springer Verlag. (cited on page 8)

Rolfsen, D., 1976. Knots and links, vol. 346. *American Mathematical Soc*, (1976). (cited on pages ix, xv, 1, 9, 10, 57, and 58)

Rosi, N. L.; Kim, J.; Eddaoudi, M.; Chen, B.; O'Keeffe, M.; and Yaghi, O. M., 2005. Rod packings and metal- organic frameworks constructed from rod-shaped secondary building units. *Journal of the American Chemical Society*, 127, 5 (2005), 1504–1518. (cited on pages xi, xv, xvii, 52, 53, 54, and 55)

Scharlemann, M., 2000. Heegaard splittings of compact 3-manifolds. *arXiv preprint math/0007144*, (2000). (cited on pages xv, 58, 59, and 60)

Tsymbal, E. Y. Section 1-crystal structure (lecture notes). *Solid-State Physics*, 927, 1–9. (cited on pages xiii and 14)

Whitehead, J., 1937. On doubled knots. *Journal of the London Mathematical Society*, 1, 1 (1937), 63–71. (cited on pages ix, 2, 57, 59, and 63)

Whitten, W., 1987. Knot complements and groups. *Topology*, 26, 1 (1987), 41–44. (cited on page 9)